2014

Static and Dynamic Error Correction of a Computer-Aided Mechanical Navigation Linkage for Arthroscopic Hip Surgery

Kangqiao Li
Bucknell University, kl030@bucknell.edu

Static and Dynamic Error Correction of a Computer-Aided Mechanical Navigation Linkage for Arthroscopic Hip Surgery

by

Kangqiao (Kristina) Li

A Thesis Submitted to the Honors Council
For Honors in Mechanical Engineering Department

April 29th, 2014

Approved by:

Emily Geist

Advisor: Emily Geist

Department Chairperson: Charles Knisely

Department Reader: Sarah Manoogian

Acknowledgements

I owe a great amount of gratitude to Professor Emily Geist. For the past two and half years, Professor Geist has provided significant and invaluable support and guidance through this project. She has inspired and motivated me to dedicate to my passion and to pursue excellence continuously. Without the endless assistance and patience of Professor Geist, this work would not have been feasible.

I would like to thank Mr. Daniel Johnson for his technical support. Thank you to Fariss Nabih (Mr. Kaguya) for his company, as well as his help on organizing my thesis. Also, my thanks go to my committee members, Professor Sarah Manoogian and Professor Erin Jablonski, for their insights, comments and suggestions. I am grateful for Professor Charles Knisely who inspired me to become an excellent and professional mechanical engineer.

Finally, the greatest appreciation and thank you goes to my family. To my parents who have been my biggest supporters, without them I would not have been able to study in the U.S. and pursue my dreams. To my grandparents who have given their most selfless love, and to my dearest friends who support me endlessly.

My four years at Bucknell University has been a great adventure, and the best part is, the journey never ends.

Table of Contents

1 List of Tables

2 List of Figures

3 Abstract

While beneficially decreasing the necessary incision size, arthroscopic hip surgery increases the surgical complexity due to loss of joint visibility. To ease such difficulty, a computer-aided mechanical navigation system was developed to present the location of the surgical tool relative to the patient's hip joint. A preliminary study reduced the position error of the tracking linkage with limited static testing trials. In this study, a correction method, including a rotational correction factor and a length correction function, was developed through more in-depth static testing. The developed correction method was then applied to additional static and dynamic testing trials to evaluate its effectiveness. For static testing, the position error decreased from an average of 0.384 inches to 0.153 inches, with an error reduction of 60.5%. Three parameters utilized to quantify error reduction of dynamic testing did not show consistent results. The vertex coordinates achieved 29.4% of error reduction, yet with large variation in the upper vertex. The triangular area error was reduced by 5.37%, however inconsistent among all five dynamic trials. Error of vertex angles increased, indicating a shape torsion using the developed correction method. While the established correction method effectively and consistently reduced position error in static testing, it did not present consistent results in dynamic trials. More dynamic paramters should be explored to quantify error reduction of dynamic testing, and more in-depth dynamic testing methodology should be conducted to further improve the accuracy of the computer-aided nagivation system.

4 Introduction

4.1 Hip arthroscopy background

Arthroscopy, as one of the most prevailing minimally invasive surgical procedures, effectively decreases the necessary incision size for joint repair operations [1]. A long thin camera, called an arthroscope, is inserted into one portal incision to display the joint area inside the patient's body. Other arthroscopic surgical tools are placed in other incision portals to complete joint repair surgeries. As shown in Figure 1, the surgeon conducts the arthroscopic procedure based merely on the camera images displayed on an operating room screen [2].

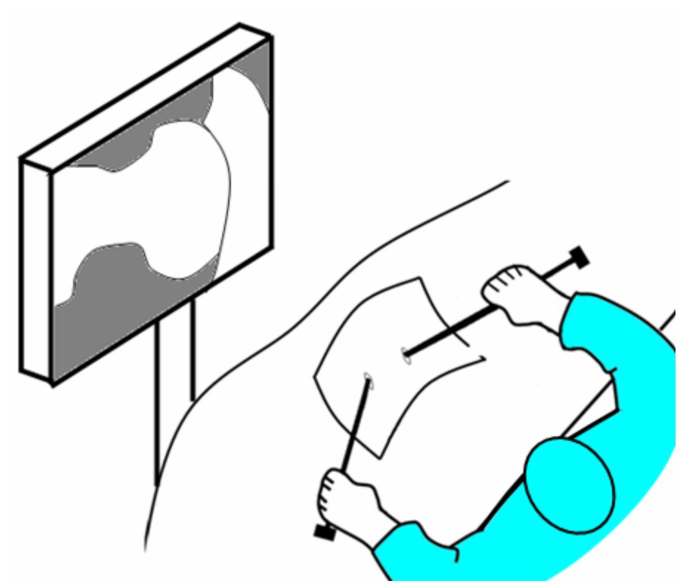

Figure 1. Standard arrangement of hip arthroscopy. An arthroscope and other surgical tools are manipulated by the surgeon through small portals placed on the patient's body [2].

While arthroscopic surgery introduces significant advantages such as shorter recovery time, less soft tissue trauma, less blood loss and a lower incidence of infection, it increases surgical complexity due to the loss of joint visibility [3]. The small incision portal limits the visibility of the joint area, and only allows the surgeon to locate areas of interest based on camera images transmitted from the arthroscope. In addition, standard arthroscopes are designed with 30° or 70° viewing angle, which further increases the difficulty of spatial orientation and navigation of the arthroscope [4]. Figure 2 shows an example of a standard arthroscope.

Figure 2. An example of current standard arthroscopes designed with 30° and 70° viewing angles [4].

As compared to knee and shoulder arthroscopy, more obstacles are encountered with hip arthroscopic surgeries. The ball and socket hip joint geometry allows for a rather tight operating envelope. Additionally, the hip joint is located relatively deeper within the body compared with the rather open operating environment for knee or shoulder. Critical nerves, veins and arteries along with ligaments and muscles are also more prominently clustered around the hip joint [5]. Therefore, it requires substantial practice, significant surgical skills and an exceptional spatial orientation for a surgeon to perform hip arthroscopic surgery.

4.2 Related work

Computer-aided techniques have been deployed commonly in recent years to assist with surgical procedures, particularly in the case of minimally invasive surgeries. In the forms of medical simulator, pre-surgery planning and intraoperative support, computer-aided systems help surgeons to improve safety, accuracy, efficiency and cost of a surgical procedure [6].

For any computer-aided minimally invasive surgery, the choice of position tracking system is of critical importance. Mechanical tracking techniques have many advantages over optical and electromagnetic tracking systems. Mechanical tracking systems avoid loss of information caused by disconnection between the optical sensors and the position receivers for optical tracking systems, and minimize the noise and distortion affected by metallic objects or stray magnetic field for electromagnetic tracking systems [7]. Nonetheless, current mechanical tracking systems are too bulky and heavy to be easily manipulated for hip arthroscopic surgeries.

A new computer-aided navigation system using a kinematically redundant mechanical tracking linkage, shown in Figure 3, is under development for hip arthroscopy [8]. The system comprises an encoder linkage for position tracking and a user interface that display both the patient anatomy and the tool position. The encoder linkage consists of eight rotational digital encoders, providing eight degrees of freedom (DOF). The extra DOF provides significant flexibility in chain motion during position tracking. With improved accuracy, the linkage along with the user interface may allow a computer-aided system to guide and assist surgeons during hip arthroscopic surgery and increase the use of arthroscopic surgeries over full incision surgeries.

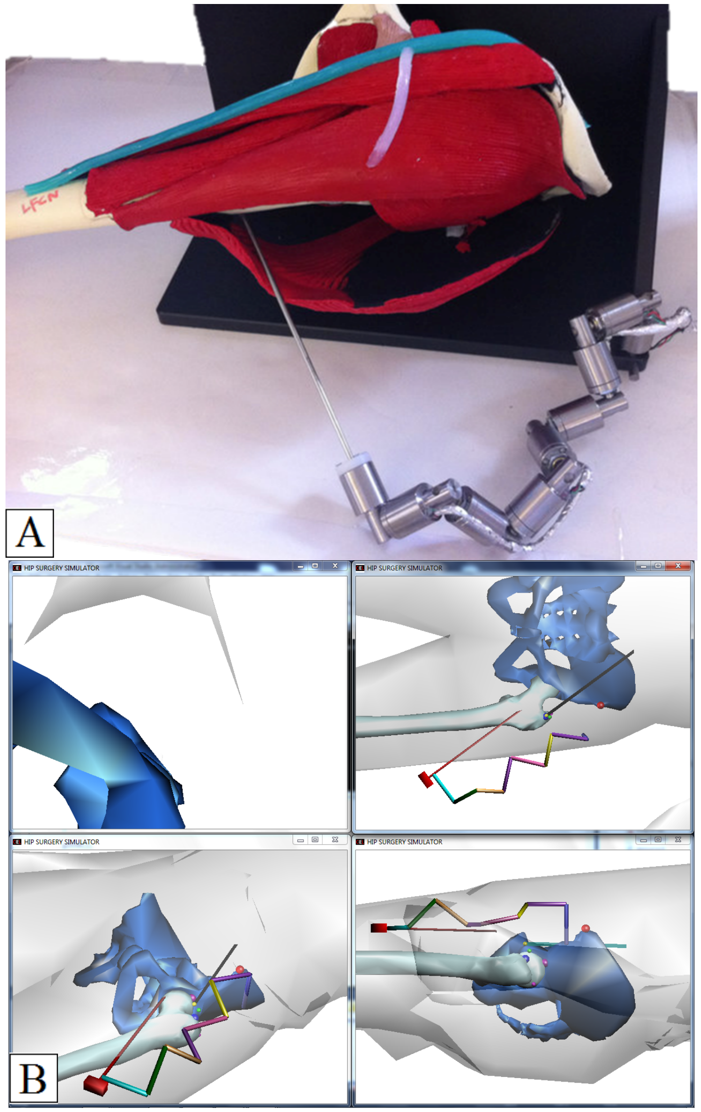

Figure 3. Computer-aided navigation system with encoder linkage applied to a hip model (A), and resulting computer display of patient geometry and tool position (B) [9].

A preliminary research study was conducted to numerically reduce the static position error in the computer-aided tracking system [9]. A testing board with nine evenly spaced holes and an isosceles triangular groove was constructed to test the accuracy of the tracking system. As shown in Figure 4, the encoder linkage was pinned at one end of the testing board. A long rod was attached at the free end of the linkage, simulating the surgical instrument in hip arthroscopy. As the surgical tool moved, the computer-aided system recorded the coordinates of the tool tip. In this research study, the nine evenly spaced holes were used, and three static numerical methods were applied to reduce the static position error of the navigation system. Preliminary results on limited trials showed that all three methods significantly reduced position error and decreased the variation in these errors.

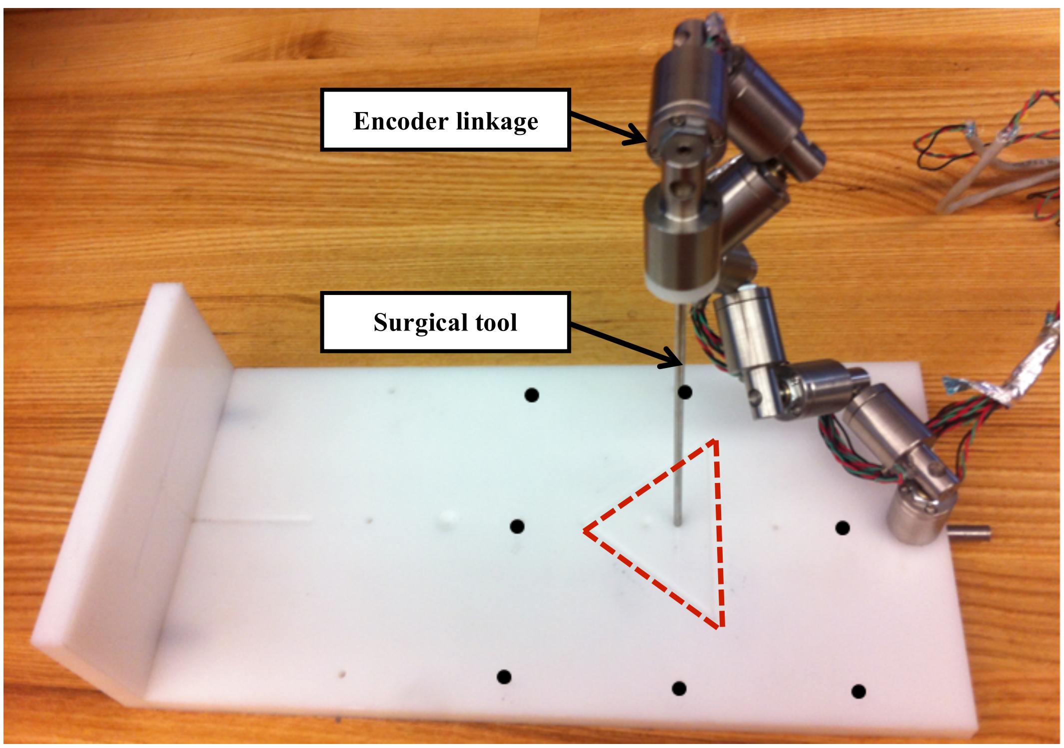

Figure 4. Testing board with nine evenly spaced holes. Rod simulating the surgical tool was inserted into the center hole [9].

4.3 Purpose of this work

During hip arthroscopic surgery, the surgical instrument is constantly moving. To evaluate the performance of the tracking system under a more realistic surgical environment, dynamic error testing is to be conducted. In addition, the scope of the previous study was limited to static error reduction over only a few trials. To further improve the accuracy of the tracking system, a more in-depth correction method that could apply to both static and dynamic testing is to be determined. More trials also need to be conducted to verify the efficiency and effectiveness of the correction method.

The objectives of this work are to 1) conduct more in-depth static testing and find a correction method to reduce the position error in the computer-aided tracking system, and 2) apply the determined correction method to static and dynamic testing trials in order to evaluate the effectiveness of this correction method.

5 Static Testing

More in-depth static testing were conducted to find a correction method to reduce the position error in the computer-aided tracking system. Ten static trials were carried out to determine the correction method. Five more static trials were conducted to evaluate the effectiveness of the developed correction method.

5.1 Correction methodology

Static testing trials were acquired and used to develop the correction method. A rotational correction factor and a length correction function were determined for static error reduction in the computer-aided navigation system.

5.1.1 Static testing data acquisition

To conduct more in-depth static testing, the testing board constructed in the previous research study was used. The nine evenly spaced holes on the testing board were utilized. The surgical instrument was placed in each known hole-position for comparison with experimental position measurements of the tracking linkage. When inserted into each hole, the surgical tool was held in place for 15 seconds to record 100 coordinate sets. In each trial, experimental position measurements of all nine holes were recorded. The average x- and y-coordinates of each hole were then calculated. Ten trials over all nine holes were completed. The averaged x- and y-coordinates of all nine holes in each trial was compared to the theoretical position of each hole. Figure 5 plots the theoretical and experimental position of all nine holes in Trial 1. Plots of other nine trials are included in Appendix A.

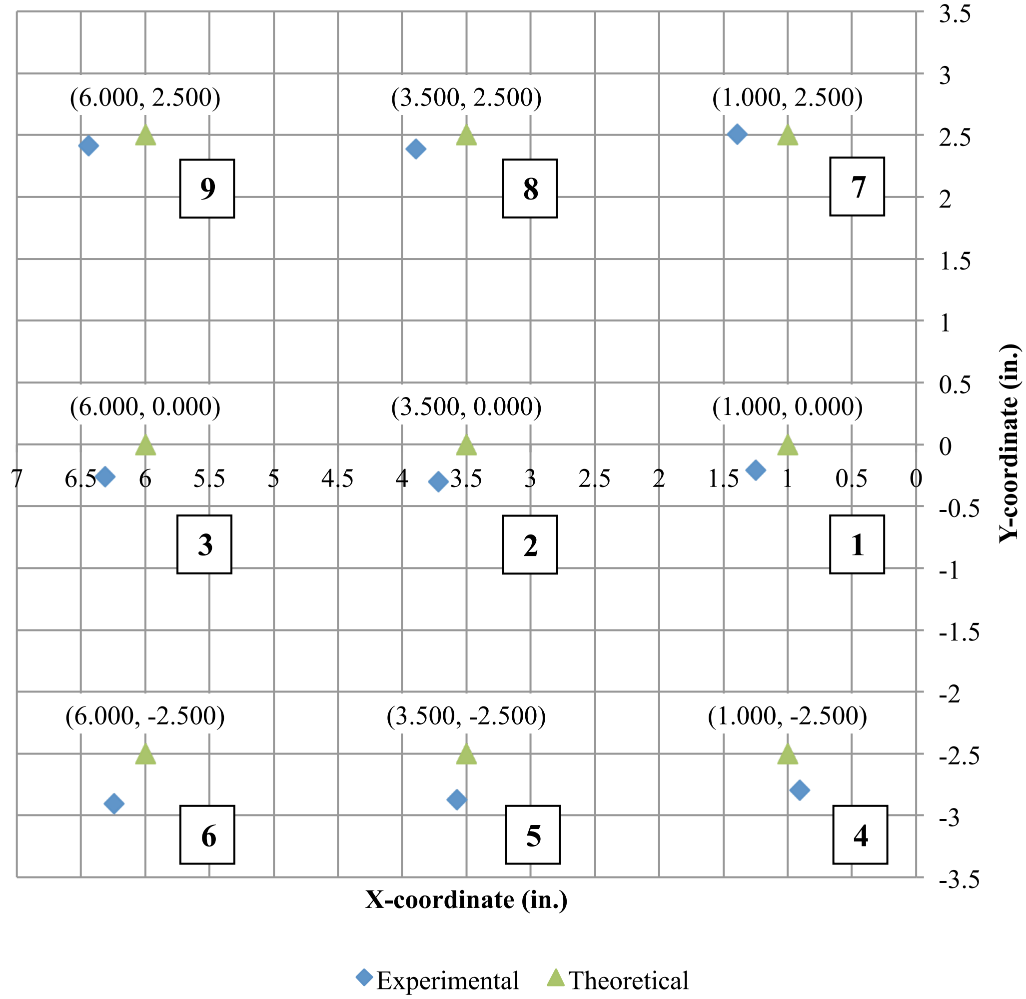

Figure 5. Plot of experimental and theoretical position of nine holes for Trial 1. Theoretical coordinates of each hole were indicated. Each hole was numbered from 1 to 9.

5.1.2 Rotational correction factor

A similar pattern was observed for all ten trials: the experimental coordinates deviated from the theoretical position in a rotational pattern around the origin. A possible cause was that position error started to accumulate and propagate through each of the eight rotational encoders in the linkage. Since one end of the linkage was pinned at the origin of the testing board, the position error reflected at the other free end was magnified.

5.1.2.1 Methodology

To reduce the rotational error, a rotational correction factor relating the experimental angle and theoretical angle was proposed. As shown in Figure 6, the theoretical point and experimental point were connected to the origin, respectively. The theoretical angle, θ_{theo}, was calculated by

$$\theta_{theo} = \tan^{-1}\left(\frac{y_{theo}}{x_{theo}}\right) \tag{1}$$

where y_{theo} is the theoretical y-coordinate of the hole location, and x_{theo} is the theoretical x-coordinate.

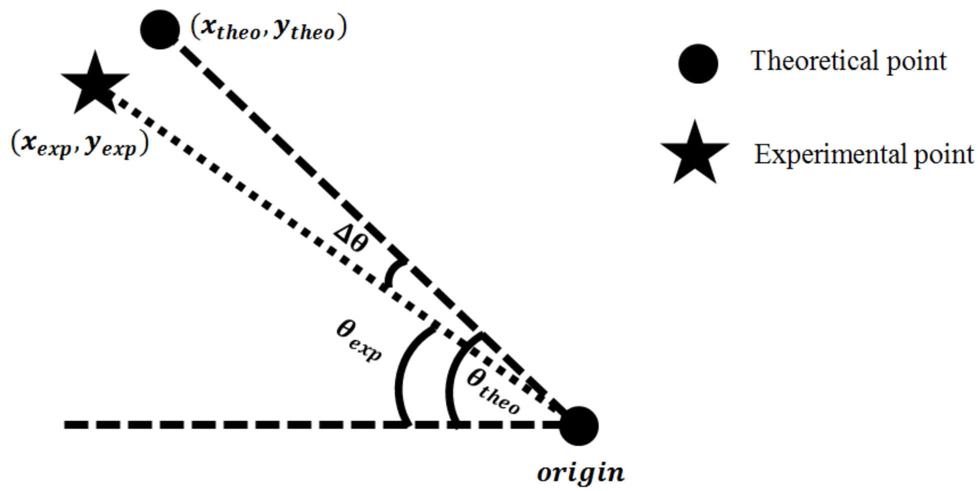

Figure 6. Schematic of determining the angle difference between theoretical angle and experimental angle for each hole location.

Similarly, the experimental angle, θ_{exp}, was calculated using

$$\theta_{exp} = \tan^{-1}\left(\frac{y_{exp}}{x_{exp}}\right) \tag{2}$$

where y_{exp} is the experimental y-coordinate of the hole location, and x_{exp} is the experimental x-coordinate. The angle difference, $\Delta\theta$, between the theoretical angle and experimental angle was determined by

$$\Delta\theta = \theta_{theo} - \theta_{exp} \tag{3}$$

The angle difference for each of the nine holes in each trial was then averaged to get the average angle difference for each trial

$$\Delta\theta_{avg,k} = \frac{1}{9}\sum_{i=1}^{9}\Delta\theta \tag{4}$$

where k = 1,2,…,10, representing the trial number, and i represented the hole number. All average angle differences in ten trials were examined and used to obtain the rotational correction factor. This examination will be discussed in the next section. The corrected angle, θ_{corr}, for each hole in each trial was then obtained by

$$\theta_{corr} = \theta_{exp} + \Delta\theta_{avg,k} \quad (5)$$

In addition, the length of segment connecting each experimental point and the origin, was calculated by

$$D_{exp} = \sqrt{{x_{theo}}^2 + {y_{theo}}^2} \quad (6)$$

In each trial, the experimental coordinates for each hole were then corrected by rotating each segment connecting the experimental point and origin by the corrected angle, using

$$x_{corr} = D_{exp} \cdot \cos\theta_{corr} \quad (7)$$

$$y_{corr} = D_{exp} \cdot \sin\theta_{corr} \quad (8)$$

To evaluate error reduction using the rotational method, the distance between the experimental point and theoretical point, d_{exp}, was compared to the distance between the corrected point and theoretical point, d_{corr}. Equations (9) and (10) and Figure 7 showed the mathematical expression and schematic of calculating d_{exp} and d_{corr}. Percent errors were determined for each hole location in each trial.

$$d_{exp} = \sqrt{\left(x_{exp} - x_{theo}\right)^2 + \left(y_{exp} - y_{theo}\right)^2} \quad (9)$$

$$d_{corr} = \sqrt{(x_{corr} - x_{theo})^2 + (y_{corr} - y_{theo})^2} \quad (10)$$

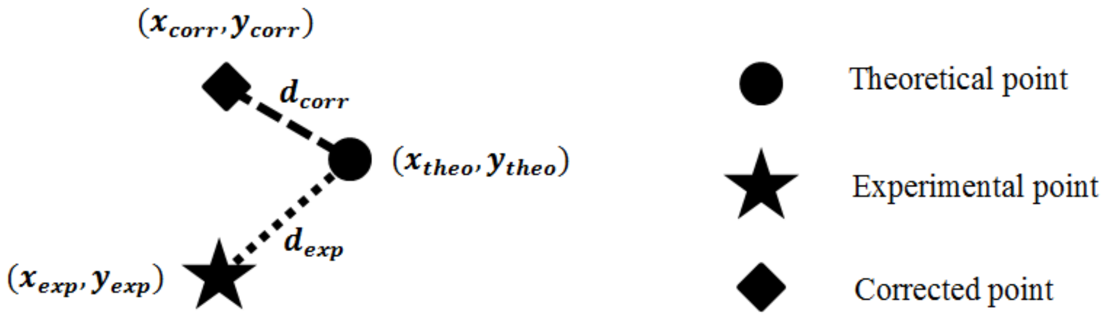

Figure 7. Schematic of determining distance between experimental point and theoretical point, and distance between corrected point and theoretical point.

5.1.2.2 Results and discussion

The distance between experimental and theoretical points and the distance between corrected and theoretical points were compared for each trial. The error reduction using the rotational method was determined for each hole in each trial. As presented in Table 1, the average error reduction in Trial 1 was 19.6%, indicating a significant error reduction result using the rotational correction method. The average error reductions in all ten trials were presented in Table 2. A consistent average error reduction of all ten trials was observed to be 23.3% with a standard deviation of 3.8%.

Table 1. Error reduction using the average angle difference for Trial 1.

Hole	Distance between experimental and theoretical points d_{exp}	Distance between corrected and theoretical points d_{corr}	Error reduction
	(in)	(in)	(%)
1	0.325	0.285	12.3%
2	0.373	0.233	37.5%
3	0.409	0.384	6.09%
4	0.311	0.247	20.5%
5	0.381	0.296	22.4%
6	0.472	0.453	3.86%
7	0.395	0.225	42.9%
8	0.409	0.266	34.9%
9	0.447	0.465	-3.91%
		Average	19.6%

Table 2. Comparison of error reduction over all nine holes using rotational correction method for all ten trials.

Trial	Error reduction
1	19.6%
2	29.5%
3	27.8%
4	24.7%
5	18.4%
6	18.8%
7	24.2%
8	21.6%
9	23.0%
10	25.7%
Average	**23.3%**
Stdev	**3.80%**

With consistent error reduction results from all ten trials, a generalized rotational correction factor was determined for later error reduction application. As seen in Table 1, the average angle difference of all ten trials presented consistency, with an average value of -0.0778 radians and standard deviation of 0.00511 radians. Due to the consistency of this average angle difference observed in all ten trials, the average value of -0.0778 was used as the rotational correction factor, θ_{CF}, for future static testing reference.

Table 3. Average angle difference in each trial.

Trial	**Average angle difference (rad)** $\boldsymbol{\Delta\theta_{avg,k}}$ **(k = 1,2,…,10)**
1	-0.0762
2	-0.0833
3	-0.0882
4	-0.0787
5	-0.0712
6	-0.0711
7	-0.0794
8	-0.0765
9	-0.0766
10	-0.0769
Average	**-0.0778**
Stdev	**0.00511**

To correct the observed rotational error in the linkage, the rotational correction factor was determined to be -0.0778 radians for future application. Using the proposed rotational method, error reduction for all ten trials remained consistent with little variation at 23.3%. As the first step of error correction, this rotational method would be applied to more trials for both static and dynamic testing in later chapters.

5.1.3 Length correction function

In addition to a rotational correction function, a length correction function was proposed and developed. As observed in Table 1, even though the average error reduction was significant, error reduction of each hole position showed large variation. The closer the hole was to the origin (holes 1, 4 and 7), the more error reduction was obtained using the rotational method. It was observed that position error increased as the hole location was further away from the origin, as seen in Figure 8.

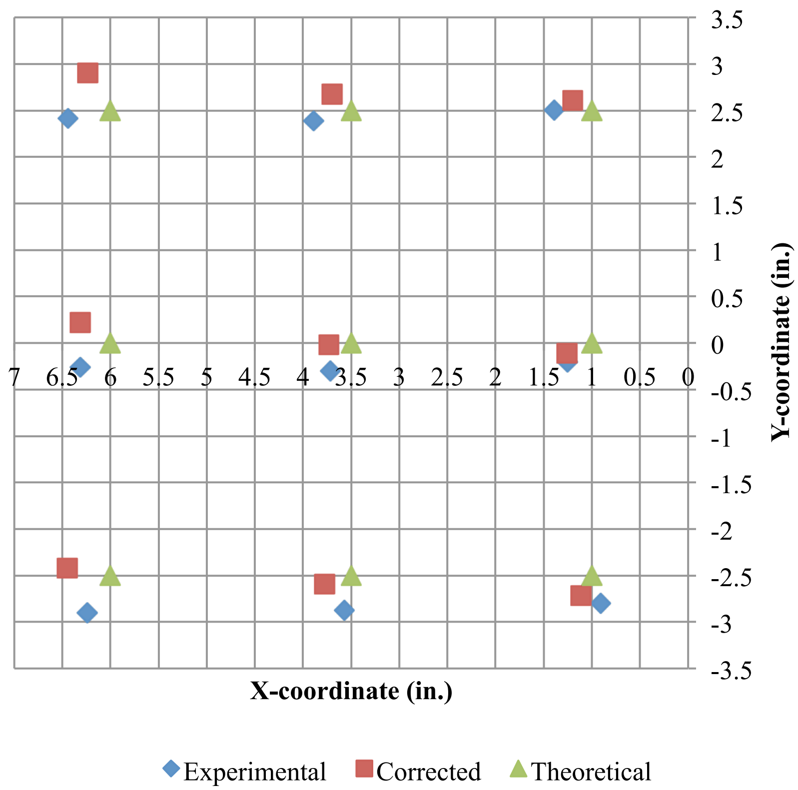

Figure 8. Plots of theoretical, experimental and corrected coordinates using rotational correction method of all nine holes for Trial 1.

5.1.3.1 Methodology

To discover the relation between the theoretical-origin distance and the experimental-origin distance, the segment length connecting the theoretical point and origin, D_{theo}, was plotted against the segment length linking the experimental point and origin, D_{exp}. Figure 9 and Equations (11) and (12) showed the schematic and mathematical expression of determining D_{theo} and D_{exp}.

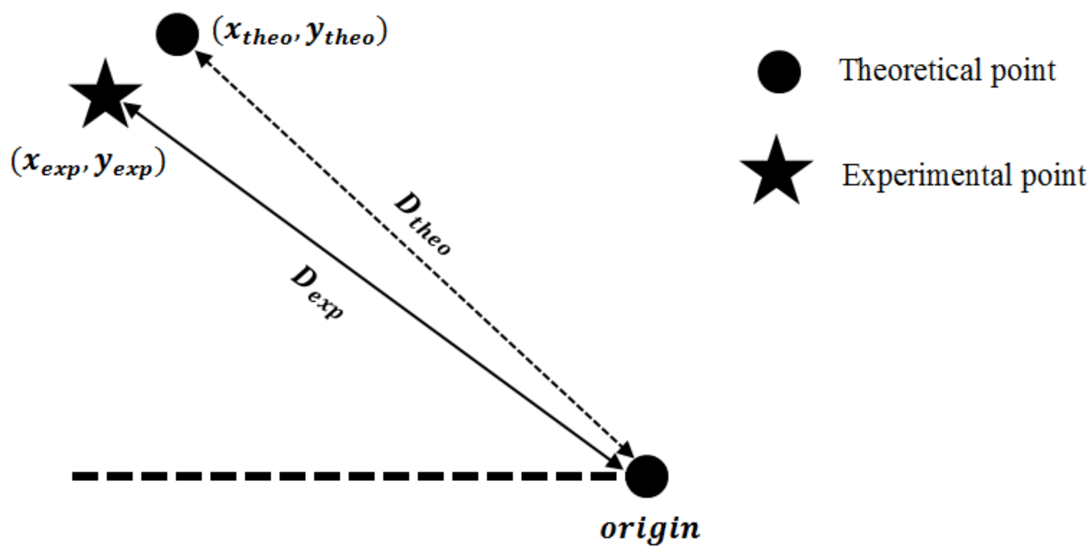

Figure 9. Schematic of determining theoretical-origin distance, and experimental-origin distance.

$$D_{theo} = \sqrt{x_{theo}{}^2 + y_{theo}{}^2} \tag{11}$$

$$D_{exp} = \sqrt{x_{exp}{}^2 + y_{exp}{}^2} \tag{12}$$

A strong correlation between the theoretical-origin distance and experimental-origin distance, with a correlation value R^2 of 0.9996, was observed in Figure 10. A strong linearity between D_{theo} and D_{exp} was therefore suggested. D_{theo} was proposed to be directly proportional to D_{exp}. A length correction function was determined by finding the linear regression line between D_{theo} and D_{exp},

$$D_{theo} = f(D_{exp}) = \boldsymbol{m}D_{exp} + \boldsymbol{b} \tag{13}$$

where m was the slope and b was the intersection. Parameters of the length correction function for all ten trials were determined. Plots to show the linear relationship between the theoretical-origin and experimental-origin distances of other nine trials are included in Appendix B.

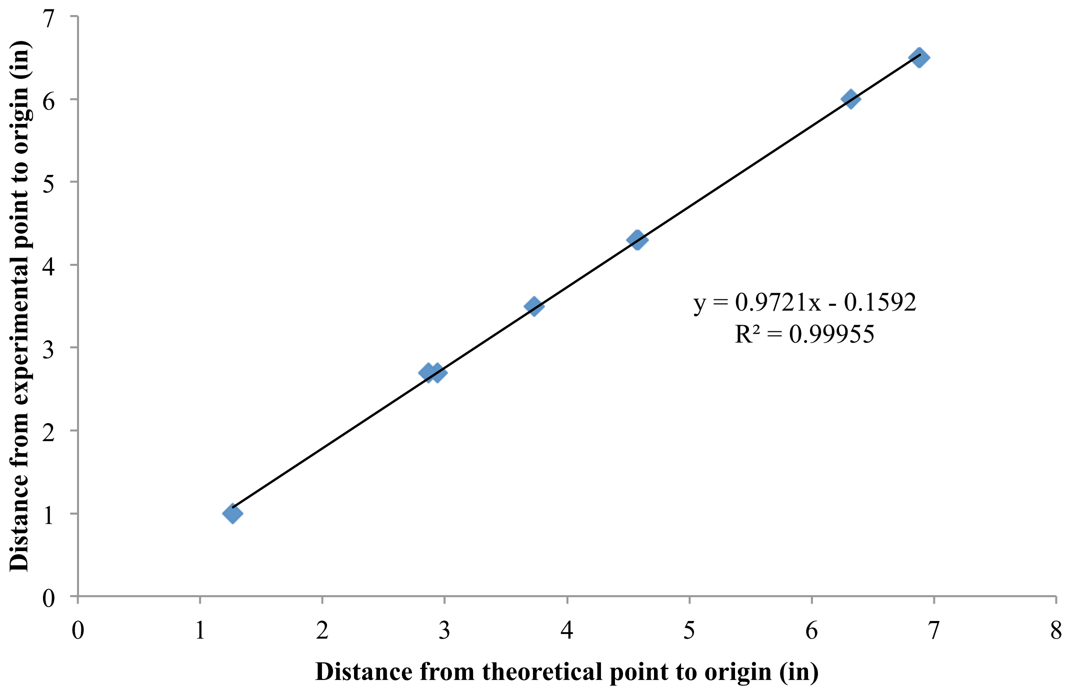

Figure 10. Plot of theoretical-origin distance and experimental-origin distance in Trial 1.

5.1.3.2 Results and discussion

The length correction function was determined for each trial and presented in Table 4. The standard deviations of each parameter remained low, which suggested consistency for all ten trials. The average values of slope and intersection were calculated and utilized as parameters of a generalized length correction for future use. The generalized length correction was shown in Equation (14).

Table 4. Slopes, intersections and correlations of for all ten trials.

Trials	Slope (m)	Intersection (b)	Correlation (R^2)
1	0.972	-0.159	0.9998
2	0.961	-0.0415	0.9995
3	0.963	-0.0775	0.9995
4	0.970	-0.108	0.9996
5	0.968	-0.122	0.9998
6	0.965	-0.108	0.9998
7	0.970	-0.130	0.9998
8	0.969	-0.140	0.9996
9	0.963	-0.077	0.9995
10	0.965	-0.079	0.9992
Average	**0.967**	**-0.104**	0.9996
Stdev	0.00370	0.0355	0.000200

$$D_{corr} = f\left(D_{exp}\right) = \mathbf{0.967}D_{exp} - \mathbf{0.104} \tag{14}$$

A linear correlation between the theoretical-origin distance and experimental-origin distance was observed. Length correction functions were calculated for all ten trials to correct the distance between experimental points and the origin. A generalized length correction function was proposed and determined for future use.

5.2 Applied methodology for static testing

Five new static testing trials were obtained to evaluate the effectiveness of the correction method. These five trials were raw coordinates data that were not used to acquire the correction factor and function. The generalized rotational correction factor and length correction function determined in previous sections were applied to the five new trials. In each trial, the length correction function was first utilized to correct the segment length connecting the experimental points and the origin, and the rotational correction factor was then used to correct the rotational error. Table 5 presents a summary of the calculated rotational correction factor and length correction function.

Table 5. Generalized rotational correction factor and length correction function.

Rotational correction factor (rad)	$\theta_{CF} = -0.778$
Length correction function (in)	$D_{corr} = 0.967D_{exp} - 0.104$

The length correction function was first applied to the five trials. In each trial, the distance between each theoretical point and origin, D_{exp}, was calculated, as discussed in Figure 7 and Equation (15). The length correction function was then applied to each experimental distance to acquire the corrected length, D_{corr}, for each hole in each trial.

The rotational correction factor was then utilized. In each trial, the experimental angle, θ_{exp}, was calculated for each hole, as presented in Figure 6 and Equation (2). The corrected angle, θ_{corr}, was obtained by

$$\theta_{corr} = \theta_{exp} + \theta_{CF} \tag{15}$$

The corrected x- and y-coordinates of each hole in each trial were then determined by rotating the corrected length by the corrected angle, expressed as

$$x_{corr} = D_{corr} \cdot \cos(\theta_{corr}) \tag{16}$$

$$y_{corr} = D_{corr} \cdot \sin(\theta_{corr}) \tag{17}$$

The position errors of the experimental coordinates, d_{exp}, and corrected coordinates, d_{corr}, were calculated using Figure 7 and Equations (9) and (10).

5.3 Results and discussion

Position errors of experimental and corrected points as well as error reduction of each hole were calculated for each trial. Table 6 presented d_{exp}, d_{corr} and error reduction of each hole in Trial 1. The average position error decreased significantly. From an average error of 0.430 inches to 0.161 inches, 62.1% of the position error was reduced in Trial 1. As seen in Figure 10, the corrected points in Trial 1 were significantly closer to the theoretical points compared with the experimental points. Results of the other four trials, included in Appendix C, also indicated consistency.

Table 6. Position errors of experimental and corrected coordinates along with error reduction in Trial 1.

Hole	d_{exp} (in)	d_{corr} (in)	Error reduction
1	0.402	0.239	40.5%
2	0.457	0.090	80.4%
3	0.496	0.135	72.7%
4	0.383	0.137	64.2%
5	0.418	0.085	79.7%
6	0.470	0.184	60.9%
7	0.377	0.247	34.5%
8	0.418	0.072	82.7%
9	0.447	0.256	42.8%
Average	**0.430**	**0.161**	**62.1%**

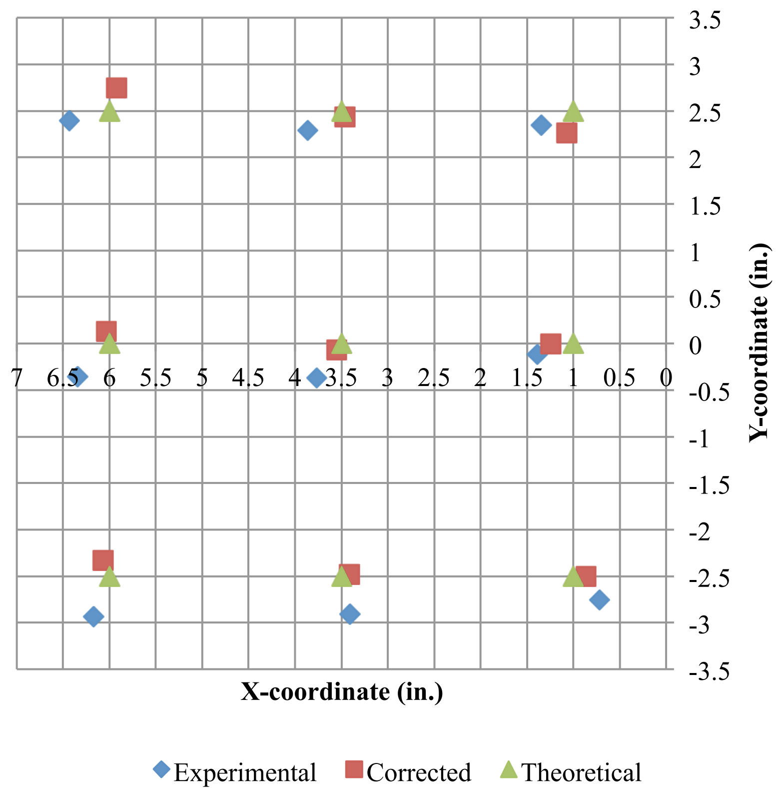

Figure 11. Plot of theoretical, experimental and corrected points using applied method in Trial 1.

The average position error of all nine holes in each trial was calculated and presented in Table 7. An average error reduction of 60.5% was observed in all five trials, which suggested that the applied correction method effectively and consistently reduced the position error in the linkage.

Table 7. Average position error of experimental and corrected coordinates along with error reduction for all ten trials.

Trial	d_{exp} **(in)**	d_{corr} **(in)**	**Error reduction**
1	0.430	0.161	62.1%
2	0.421	0.143	65.4%
3	0.359	0.156	54.0%
4	0.395	0.156	60.4%
5	0.364	0.148	60.7%
Average	**0.394**	**0.153**	**60.5%**

6 Dynamic Testing

To simulate a more realistic surgical situation when the surgical instrument is constantly moving during arthroscopic hip surgery, dynamic testing trials were conducted. The correction method developed in previous chapter was applied to the dynamic trials to evaluate its effectiveness.

6.1 Dynamic testing data acquisition

For dynamic testing, the triangular groove on the testing board was used to record dynamic testing data. As shown in Figure 12, the upper, lower and mid-points were the three vertices of the triangle; the upper, lower and vertical lines were the three sliding channels. Starting from the lower point, the surgical instrument slid through the three channels continuously and ended at the starting point. Coordinates of the tool tip were recorded in the computer-aided system and utilized for error reduction. Five dynamic testing trials were conducted.

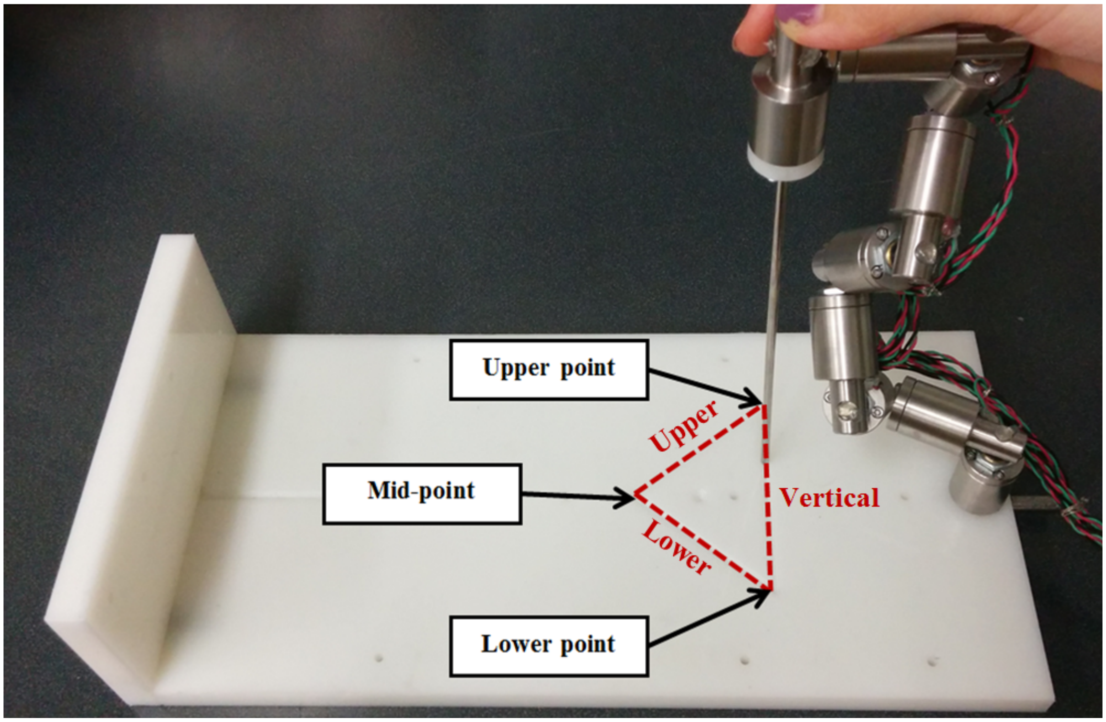

Figure 12. Dynamic testing using the triangular groove on testing board. The surgical tool was sliding through the groove to record position coordinates.

6.2 Applied methodology for dynamic testing

The rotational correction factor and length correction function developed in the static testing section were applied to dynamic testing data in order to reduce position error when the tool was moving. The same correction procedure in the static testing section was utilized. The corrected coordinates in each trial were then plotted to show trace of the corrected triangle.

Different from the known hole locations in static testing, it was difficult to quantitatively determine error reduction in dynamic testing. Several methods were used to quantify parameters that could be compared to show improvement of accuracy.

First, linear regression lines of the three channels of both experimental and corrected triangle were determined to calculate coordinates of the triangle vertices. The distance between the experimental and theoretical vertices was then compared with the distance between the corrected and theoretical vertices.

Second, areas of the experimental and corrected triangles were compared with the area of the theoretical triangle, respectively. Vertices of the experimental and corrected triangles found in the preceding paragraph were used to calculate the triangular areas. The area of a triangle given vertex coordinates were determined by

$$S = \frac{1}{2} \cdot [x_1(y_2 - y_3) + x_2(y_3 - y_1) + x_3(y_1 - y_2)] \tag{18}$$

where S was the area, (x_1, y_1), (x_2, y_2) and (x_3, y_3) were the vertex coordinates.

Additionally, vertex angles formed by the regression lines of both experimental and corrected triangles were compared with the theoretical vertex angles, respectively. Slopes of the regression lines calculated in the preceding section were used to calculated vertex angles. The vertex angle of a triangle given slopes were determined using

$$\alpha_1 = \tan^{-1} m_2 + \tan^{-1} m_3 \tag{19}$$

where $\alpha_1$was the vertex angle, m_2 and m_3 were slopes of the neighboring sides. A schematic of determining the vertex angle was shown in Figure 13.

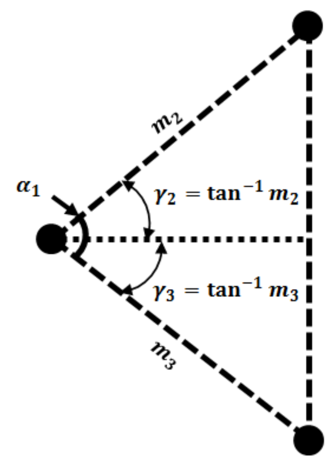

Figure 13. Schematic of determining the vertex angle given slopes of its neighboring sides.

Finally, visual examination of the experimental and corrected triangles was conducted. General observations such as shape and closeness of each triangular side were carried out to qualitatively determine the effectiveness of the correction method in dynamic testing.

6.3 Results and discussion

Differences between experimental and theoretical vertices in each dynamic testing trial were compared to the distances between corrected and theoretical vertices. As presented in Table 8 and Table 9, an average vertex location error reduction of 29.4% was achieved. Error reductions of the lower vertices in all five trials were consistent, with 65.1% reduction and standard deviation of 7.90%. Mid-vertices also witnessed consistent error reduction with an average of 39.1% for all five trials. However, an increase of average vertex position error was observed for the upper vertices. Standard deviation of

35.6% of the upper vertices error difference indicated inconsistency of the upper vertices in the five trials. More specifically, the upper point in trials 2, 3 and 4, error of the vertex locations increased after the correction method was applied. In trials 1 and 5, error reductions of the upper vertex (26.9% and 0.200%, respectively) were also lower than the lower and mid-points in the same trials (each error reduction more than 45%). In addition, the error reduction of the lower point in each trial was always the highest compared to that of the upper and mid-points.

Table 8. Comparison between experimental and corrected vertex distances from theoretical vertex locations.

Trial	**Vertex**	**Experimental (in)**	**Corrected (in)**	**Reduced distance (in)**	**Error reduction %**	**Average reduction %**
1	**Lower**	0.257	0.112	0.144	56.2%	43.1%
	Upper	0.316	0.231	0.085	26.9%	
	Mid	0.326	0.176	0.150	46.1%	
2	**Lower**	0.392	0.138	0.254	64.7%	10.9%
	Upper	0.212	0.301	-0.089	-41.9%	
	Mid	0.270	0.243	0.026	9.7%	
3	**Lower**	0.330	0.123	0.207	62.8%	35.7%
	Upper	0.275	0.284	-0.008	-3.0%	
	Mid	0.341	0.179	0.161	47.4%	
4	**Lower**	0.346	0.125	0.221	63.9%	11.7%
	Upper	0.169	0.274	-0.105	-62.2%	
	Mid	0.289	0.192	0.097	33.5%	
5	**Lower**	0.386	0.086	0.301	77.8%	45.6%
	Upper	0.238	0.238	0.000	0.200%	
	Mid	0.342	0.141	0.201	58.8%	
					Average	**29.4%**

Table 9. Average error reduction and standard deviation of all five dynamic testing trials.

Vertex	Average error reduction	Stdev
Lower	65.1%	7.90%
Upper	-16.0%	35.6%
Mid	39.1%	18.7%

Areas of the experimental and corrected triangles were compared with theoretical triangular area. Table 10 presented the theoretical, experimental and corrected areas of all five trials. The experimental triangular areas were all greater than the theoreatical areas. After the correction method was applied, the corrected areas were lower than the experimental values. For Trials 2, 4 and 5, triangular areas after correction indicated consistent error reduction of the triangular area. Trial 2 also suggested improvement in triangular area. Trial 1, on the other hand, showed an increase in error of the corrected triangular area. During the dynamic testing, speed of the surgical instrument was not controlled. This could result in a large variation in the experimental coordinates, thus the experimental triangular areas.

Table 10. Comparison of theoretical, experimental and corrected triangular areas of all five dynamic testing trials.

Trial	Theoretical area (in^2)	Experimental area (in^2)	Corrected area (in^2)	Experimental error	Corrected error	Reduced error
1	3.000	3.008	2.732	0.260%	8.94%	-8.68%
2	3.000	3.309	2.998	10.3%	0.0700%	10.2%
3	3.000	3.210	2.912	7.01%	2.94%	4.07%
4	3.000	3.412	3.092	13.7%	3.07%	10.7%
5	3.000	3.421	3.103	14.0%	3.43%	10.6%
Average	3.000	3.272	2.967	**9.06%**	**3.69%**	**5.37%**

Vertex angles bounded by regression lines of both experimental and corrected triangles were compared with the theoretical vertex angles. As shown in Table 11, vertex angles of experimental triangles suggested little error. Average experimental errors of all five trials for lower, upper and mid-points were 6.40%, 1.73% and 1.48% , respectively. However, average corrected errors for lower, upper and mid-points were 10.7%, 3.00% and 3.07%, respectively. An increase in vertex angle error was observed in the corrected data. This error increase suggested that the shape of triangle was subject to distortion after the correction method was applied.

Table 11. Experimental and corrected errors of vertex angles in all five trials.

Trial		1	2	3	4	5	Average
Lower point	**Experimental error**	7.53%	5.13%	8.23%	5.63%	5.51%	6.40%
	Corrected error	11.5%	12.7%	8.12%	10.4%	10.9%	10.7%
Upper point	**Experimental error**	0.160%	4.75%	0.190%	1.54%	2.02%	1.73%
	Corrected error	0.0500%	2.47%	3.80%	3.77%	4.93%	3.00%
Mid point	**Experimental error**	1.43%	0.940%	2.26%	1.01%	1.75%	1.48%
	Corrected error	3.42%	1.02%	4.24%	2.97%	3.69%	3.07%

In addition, the shapes of experimental and corrected triangles were visually inspected. Figure 14 plots the theoretical, experimental and corrected triangles in Trial 2. Plots of the other four trials are included in Appendix D. As observed in Figure 14, the corrected triangle was closer to the theoretical triangle in terms of vertex locations and distance between respective triangular sides. This was examined through the vertex coordinates in a previous section. Additionally, the three sides of the experimental triangle presented a parallel relationship with the sides of the theoretical triangle. The upper channel was observed to shift downward as compared to the theoretical upper channel. The lower channel indicated the same shifting pattern with a longer shift distance. The experimental vertical channel was not completely linear, yet deviating closely around the theoretical vertical channel. The shifting pattern was not observed or accounted for in the static testing trials. It would be beneficial to further explore this shifting pattern and incorporate it into the universal correction method.

The corrected triangle was then compared to the theoretical triangle. The corrected lower vertex was significantly closer to the theoretical vertex location compared with the experimental location. The three sides of the corrected triangle, however, lost the parallel relationship with the theoretical triangle observed before the correction method was applied. The correction method included a rotational correction as well as a length correction. While the length correction shrank the triangle, the rotational correction resulted in over-rotation of the triangle. For future work, the angle formed between each corrected and theoretical channel could be examined to see if the over-rotation was consistent for all three channels. This angle value could be incorporated into the rotational method if the angle values were found consistent.

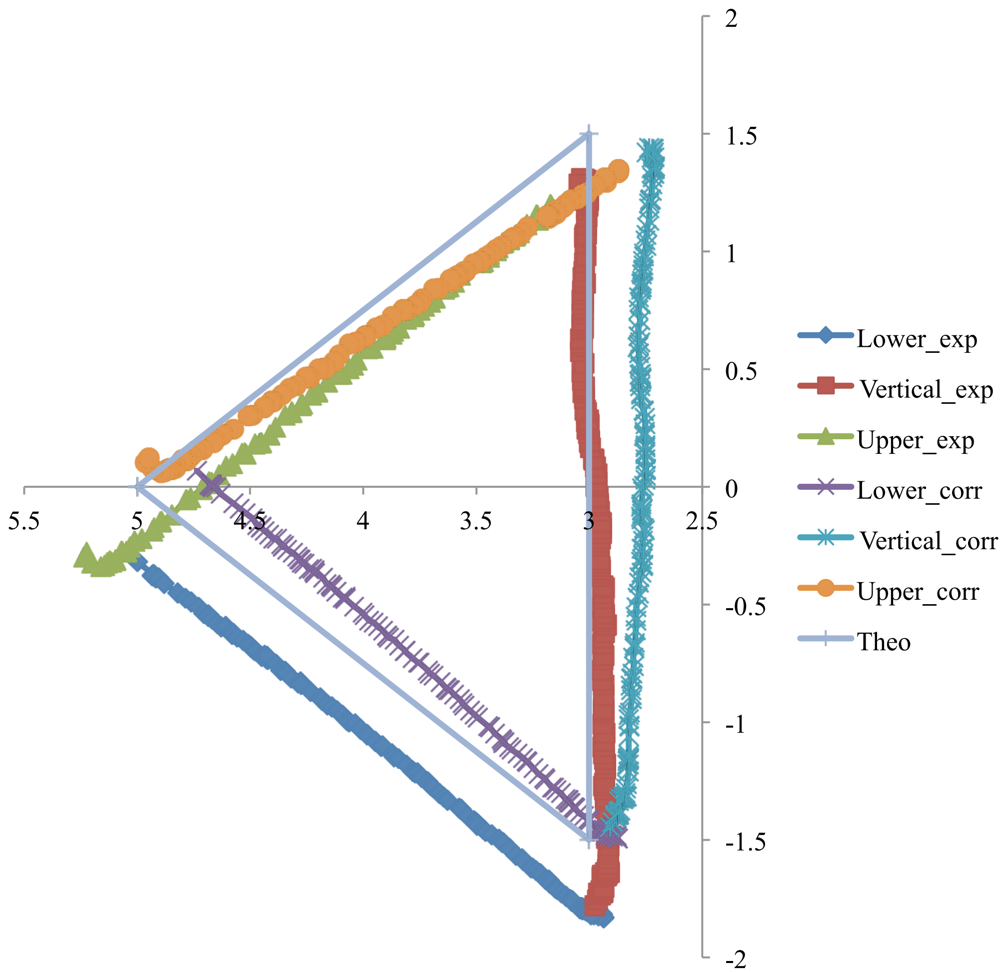

Figure 14. Plot of theoretical, experimental and theoretical triangles for dynamic testing in Trial 2.

In conclusion, as compared to static testing, it was difficult to quantify the effectiveness of the correction method for dynamic testing. Error reductions regarding vertex positions, vertex angles and triangular areas were determined. The results proved to be inconsistent for the limited trials conducted for dynamic testing. The correction method developed in static testing might not be the most effective way to reduce error in dynamic testing.

7 Conclusions

To reduce the position error in a computer-aided tracking system for hip arthroscopic surgery, a correction method that utilized a rotational correction factor and a length correction function was developed from static testing trials. The rotational correction factor and the length correction function were applied to more static testing trials to evaluate the effectiveness of this correction method. Position error for the additional static testing trials was reduced significantly, indicating that the determined correction method was effective to improve the system accuracy.

In addition, dynamic testing was conducted to simulate a more realistic surgical environment in which the surgical instrument is constantly moving. The same correction method was applied to dynamic testing trials. Three parameters including vertex location, vertex angle and triangular area were utilized to quantify the error reduction in dynamic testing. Performance of the correction method suggested inconsistent error reduction results in dynamic testing.

For future work, additional dynamic testing trials are to be conducted to evaluate the effectiveness of the developed correction method. More parameters in dynamic testing are subject to development to quantify error reduction in the moving tracking linkage. More in-depth dynamic error reduction procedures and methods are to be determined.

8 Future Work

To further improve the accuracy of the computer-aided navigation system, more in-depth exploration on dynamic correction needs to be conducted. In this study, three quantitative parameters, including the vertex coordinates, vertex angles and triangular areas, were determined to evaluate the position error reduction of the tracking linkage in dynamic testing. The performances of these parameter evaluation, however, were not consistent or effective. More appropriate parameters to quantify the dynamic error reduction should be developed to provide more efficient evaluation of the correction method. Also, more dynamic testing should be conducted in addition to the five dynamic trials carried out in this study. To reduce the inconsistency presented in each dynamic trial, a mechanism or device designed to control the speed of the moving surgical instrument would be advantageous in minimizing any irregular movement of the tool tip. Additionally, it would be beneficial to incorporate the shift parttern observed in the five dynamic testing trials into the correction method. Other dynamic testing procedures could be explored as well to simulate a more realistic operating envelope required for arthroscopic hip surgery.

Bibliography

1. Berger, R. A., & Tria Jr., A. J. (2012). *Minimally Invasive Surgery for Unicondylar Knee Arthroplasty: The Intramedullary Technique.* New York: Springer Science+Business Media.
2. Geist, E. M. (2007). *Computer-Adied Navigation System for Arthroscopic Hip Surgery.* Pittsburgh: Carnegie Mellon University.
3. Safran, M. R., Stone, D. A., & Zachazewski, J. E. (2003). *Instructions for sports medicine patients.* Philadelphia: Saunders.
4. Stryker. (n.d.). *Standardization with Clarity.* Retrieved April 5, 2014, from Arthroscopes Brochure: https://www.stryker.com/stellent/groups/public/documents/web_prod/030197.pdf
5. Kelly, T. B., Williams, J. R., & Philippon, J. M. (2003). Hip Arthroscopy: Current Indications, Treatment Options, and Management Issues. *The American Journal of Sports Medicine, 31*(6), 1020-1037.
6. Joskowicz, L., & Taylor, R. (2001). Computers in imaging and guided surgery. *Computing in Science & Engineering, 3*(5), 65-72.
7. Birkfellner, W., Watzinger, F., Wanschitz, F., Ewers, R., & Bergmann, H. (1998). Calibration of tracking systems in a surgical environment. *Medical Imaging, IEEE Transactions on, 17*(5), 737-742.
8. Monahan (Geist), E., & Shimada, K. (2006). Computer-aided navigation. *Int J Med Robotics Comput Assist Surg, 2*(3), 271-278.

9. Li, K., & Geist, E. M. (2013). Numerical Correction of Error in A Computer-Aided Mechanical Navigation System for Arhtroscopic Hip Surgery. Washington: American Society of Mechanical Engineers.

Appendices

Appendix A. Plots of experimental points for static testing.

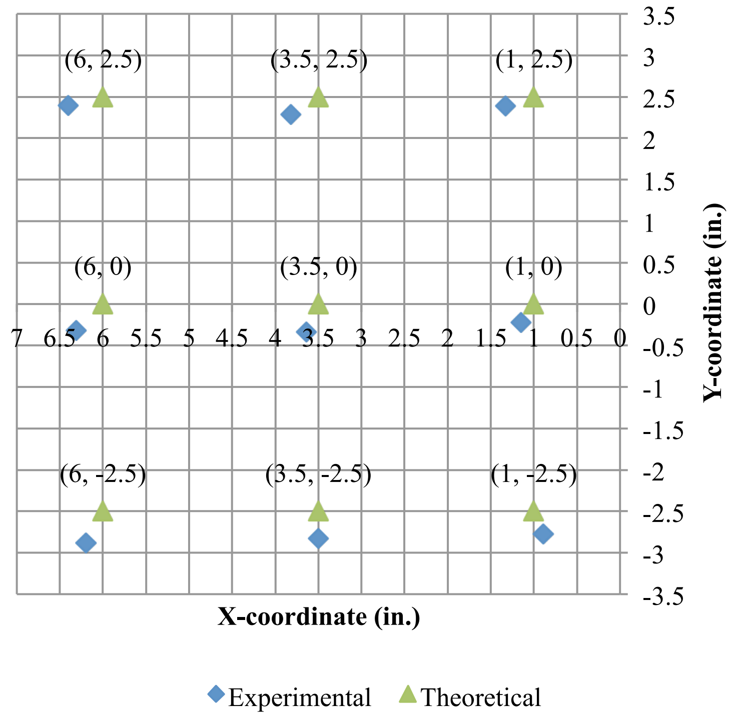

Figure A 1. Plot of experiment and theoretical points in Trial 2 for static testing.

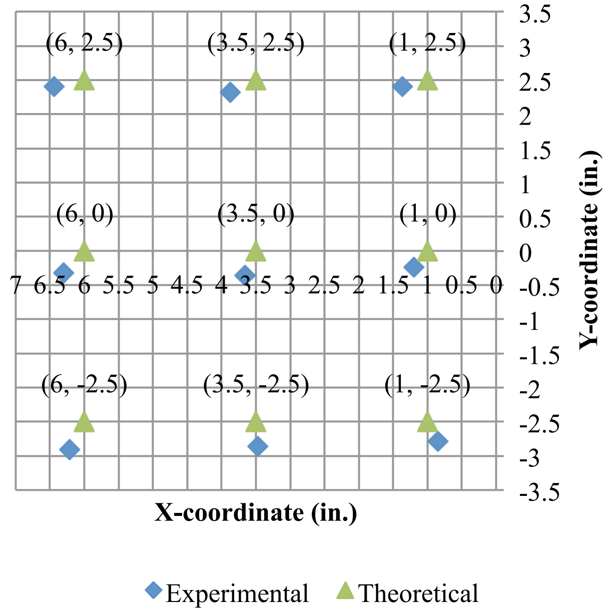

Figure A 2. Plot of experiment and theoretical points in Trial 3 for static testing.

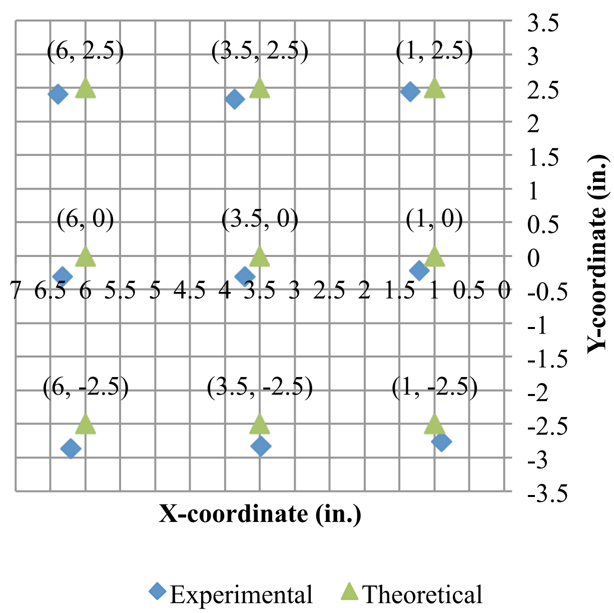

Figure A 3. Plot of experiment and theoretical points in Trial 4 for static testing.

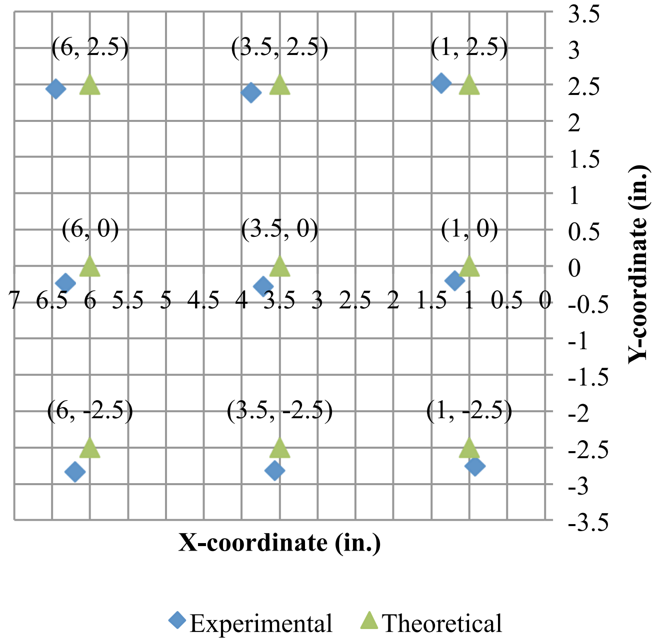

Figure A 4. Plot of experiment and theoretical points in Trial 5 for static testing.

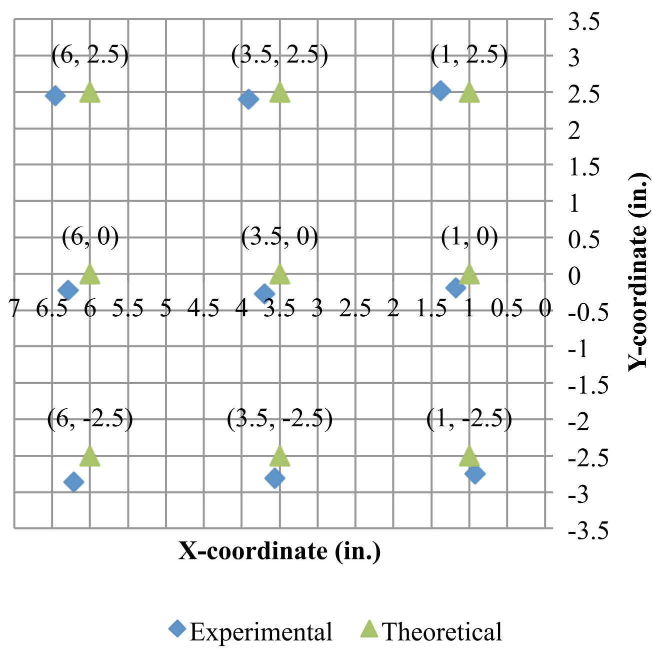

Figure A 5. Plot of experiment and theoretical points in Trial 6 for static testing.

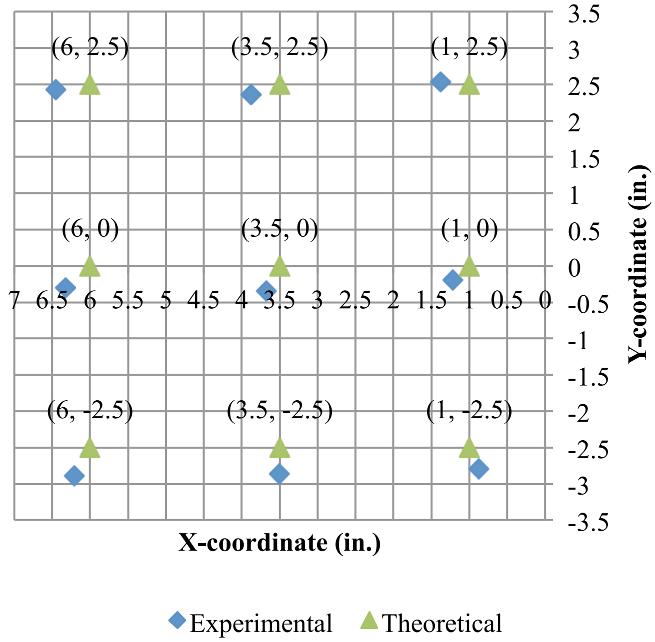

Figure A 6. Plot of experiment and theoretical points in Trial 7 for static testing.

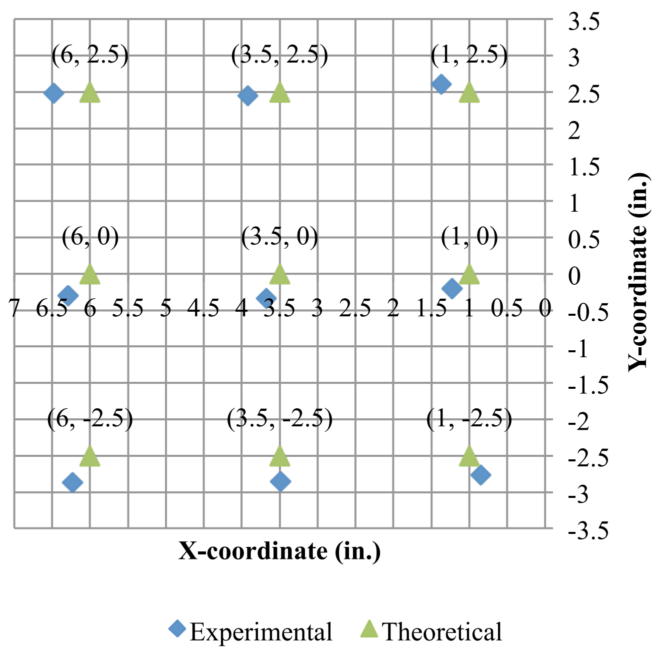

Figure A 7. Plot of experiment and theoretical points in Trial 7 for static testing.

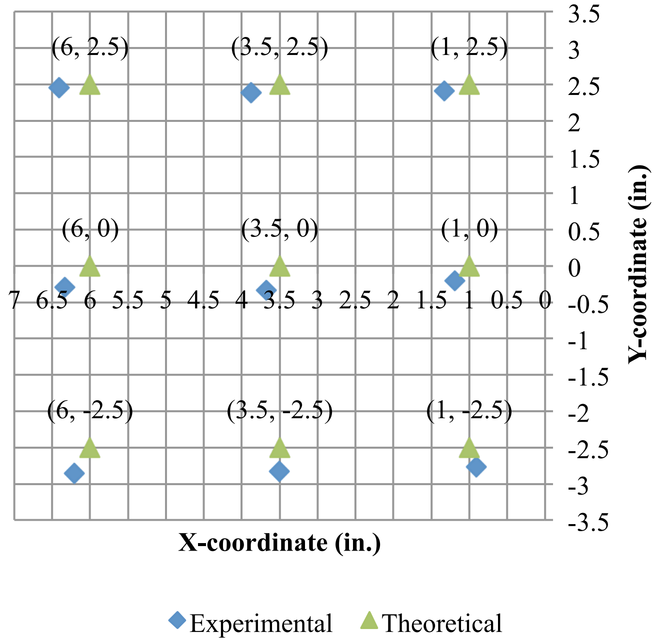

Figure A 8. Plot of experiment and theoretical points in Trial 9 for static testing.

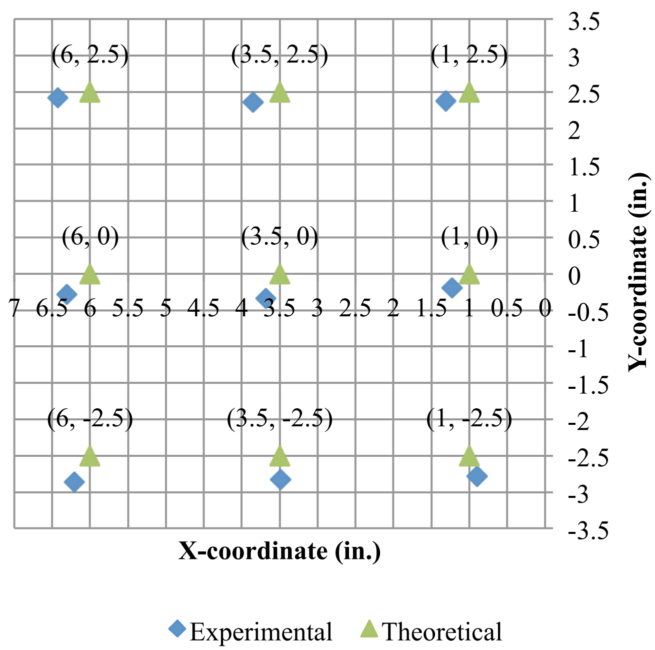

Figure A 9. Plot of experiment and theoretical points in Trial 10 for static testing.

Appendix B. Plots of linear distance relationship for static testing.

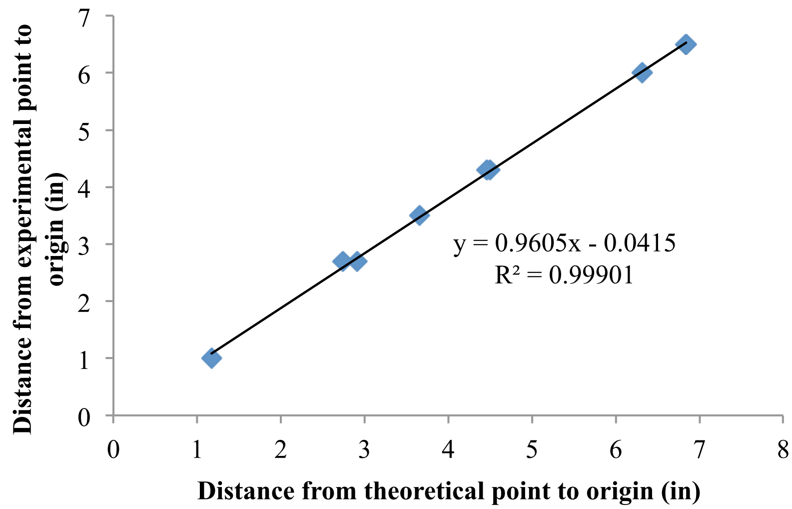

Figure B 1. Plot of theoretical-origin distance and experimental-origin distance in Trial 2.

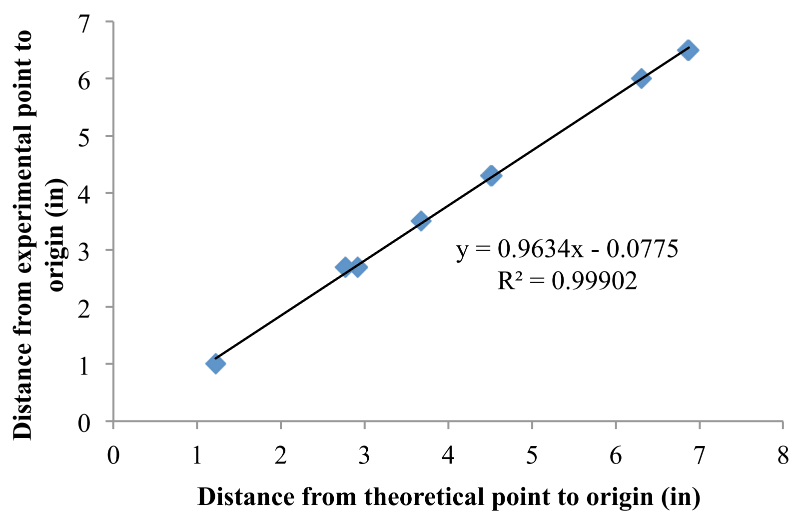

Figure B 2. Plot of theoretical-origin distance and experimental-origin distance in Trial 3.

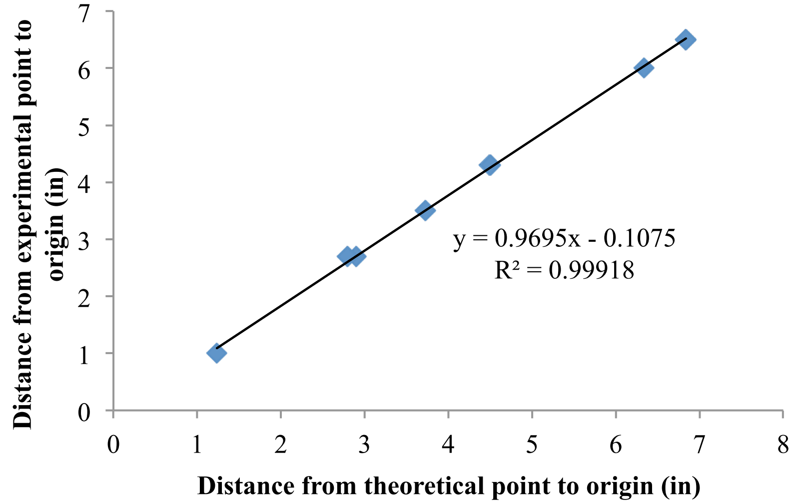

Figure B 3. Plot of theoretical-origin distance and experimental-origin distance in Trial 4.

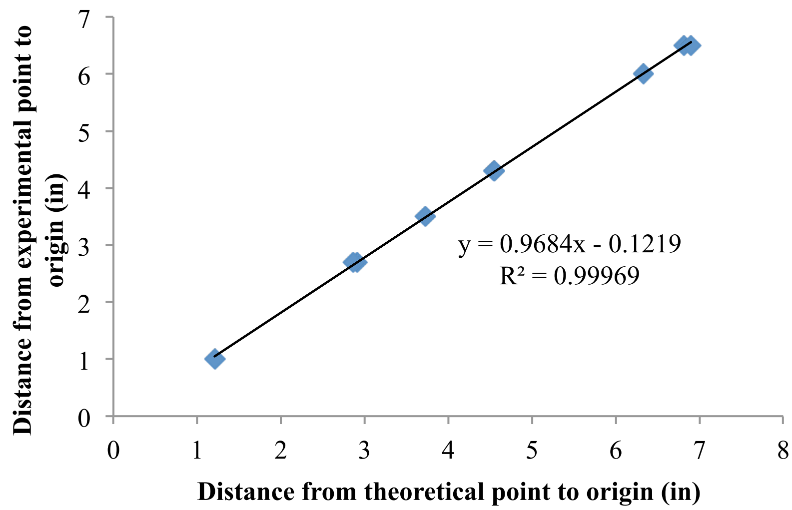

Figure B 4. Plot of theoretical-origin distance and experimental-origin distance in Trial 5.

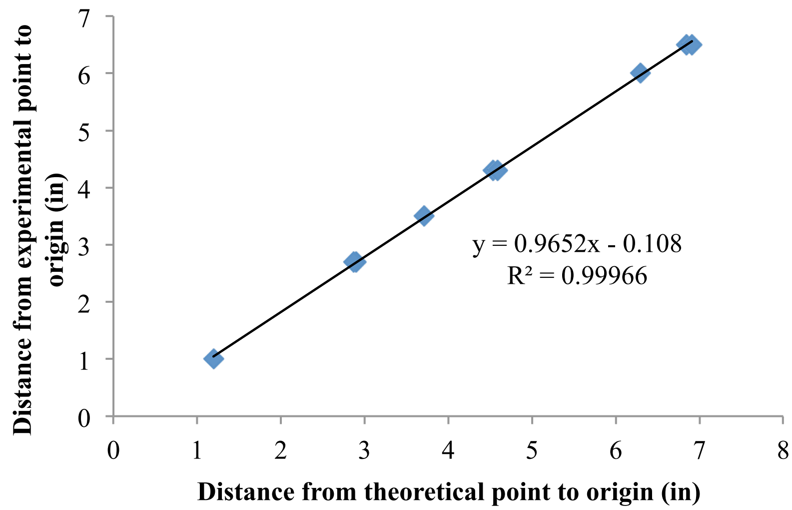

Figure B 5. Plot of theoretical-origin distance and experimental-origin distance in Trial 6.

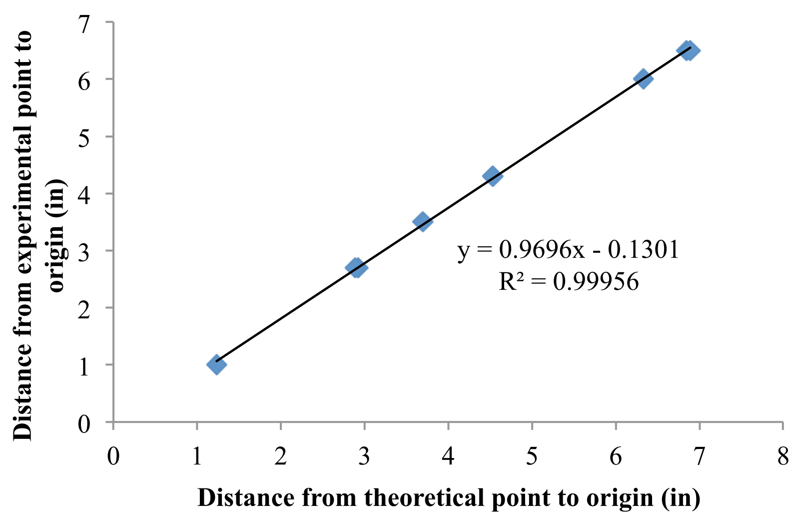

Figure B 6. Plot of theoretical-origin distance and experimental-origin distance in Trial 7.

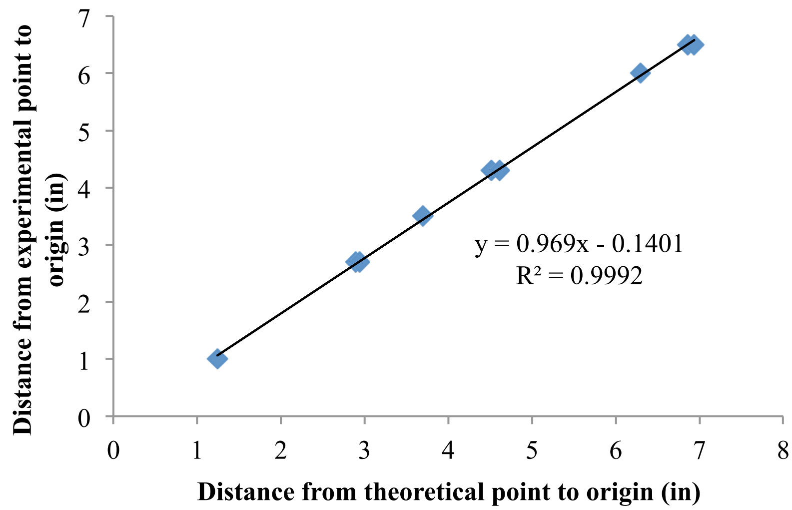

Figure B 7. Plot of theoretical-origin distance and experimental-origin distance in Trial 8.

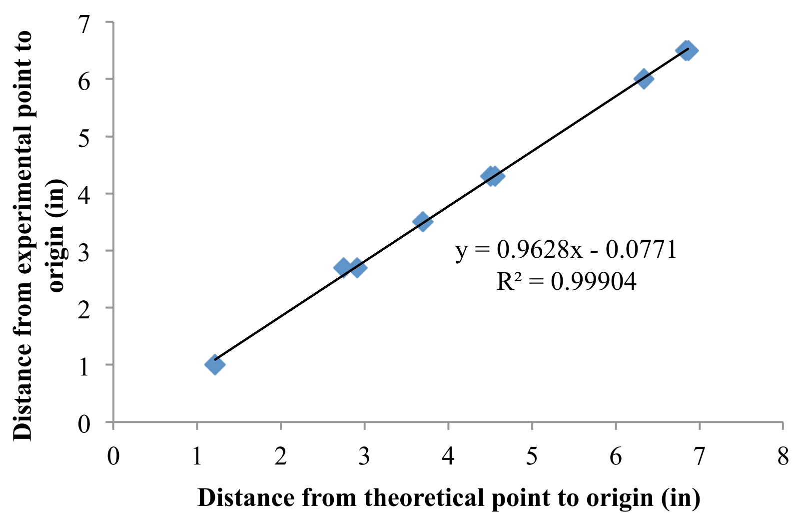

Figure B 8. Plot of theoretical-origin distance and experimental-origin distance in Trial 9.

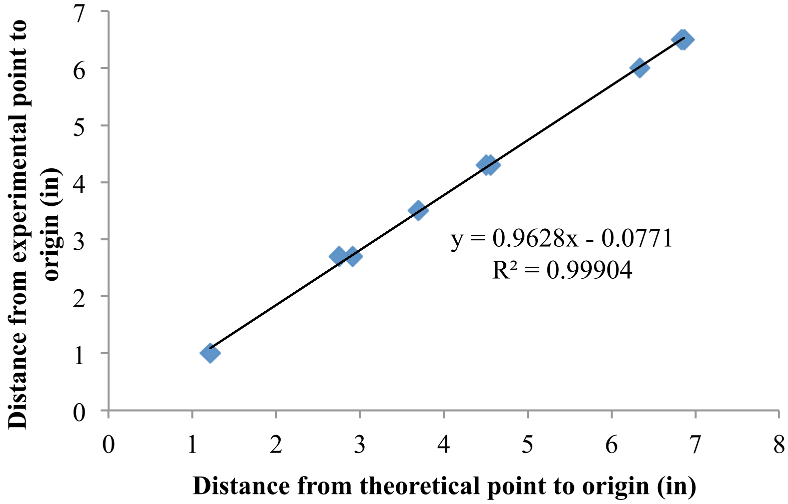

Figure B 9. Plot of theoretical-origin distance and experimental-origin distance in Trial 10.

Appendix C. Results of applied correction method for static testing.

Table C 1. Position errors of experimental and corrected coordinates along with error reduction in Trial 2.

Hole	d_{exp} (in)	d_{corr} (in)	Error reduction
1	0.353	0.194	45.1%
2	0.443	0.099	77.7%
3	0.478	0.127	73.5%
4	0.368	0.088	76.2%
5	0.408	0.071	82.7%
6	0.479	0.202	57.9%
7	0.340	0.222	34.7%
8	0.437	0.009	97.9%
9	0.484	0.276	42.9%
Average	0.421	0.143	65.4%

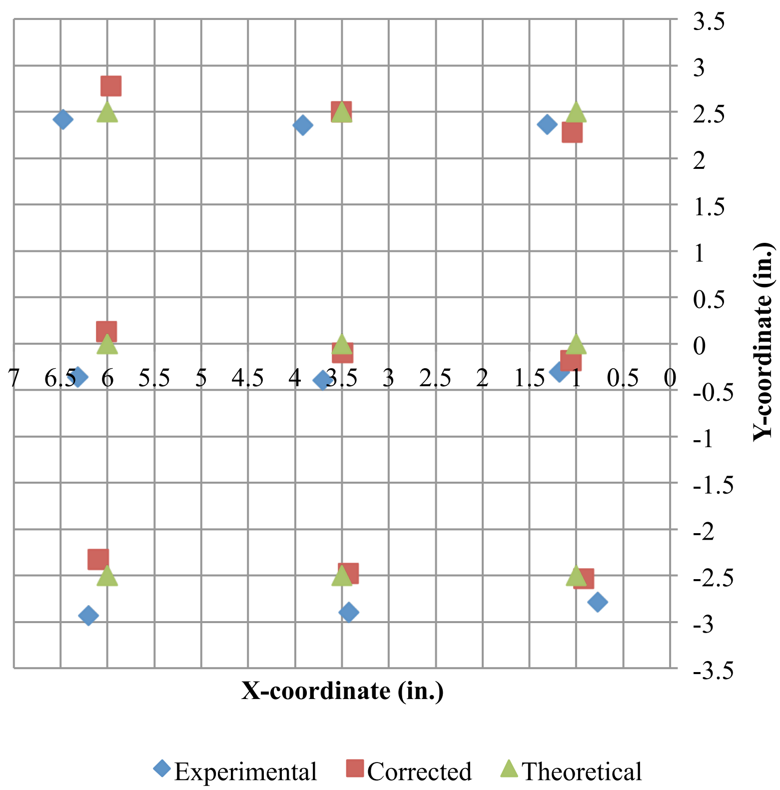

Figure C 1. Plot of theoretical, experimental and corrected points using applied method in Trial 2.

Table C 2. Position errors of experimental and corrected coordinates along with error reduction in Trial 3.

Hole	d_{exp} (in)	d_{corr} (in)	Error reduction
1	0.328	0.170	48.1%
2	0.358	0.004	98.8%
3	0.381	0.192	49.7%
4	0.207	0.094	54.7%
5	0.221	0.199	10.0%
6	0.400	0.228	43.1%
7	0.350	0.199	43.2%
8	0.460	0.030	93.6%
9	0.523	0.288	44.9%
Average	0.359	0.156	54.0%

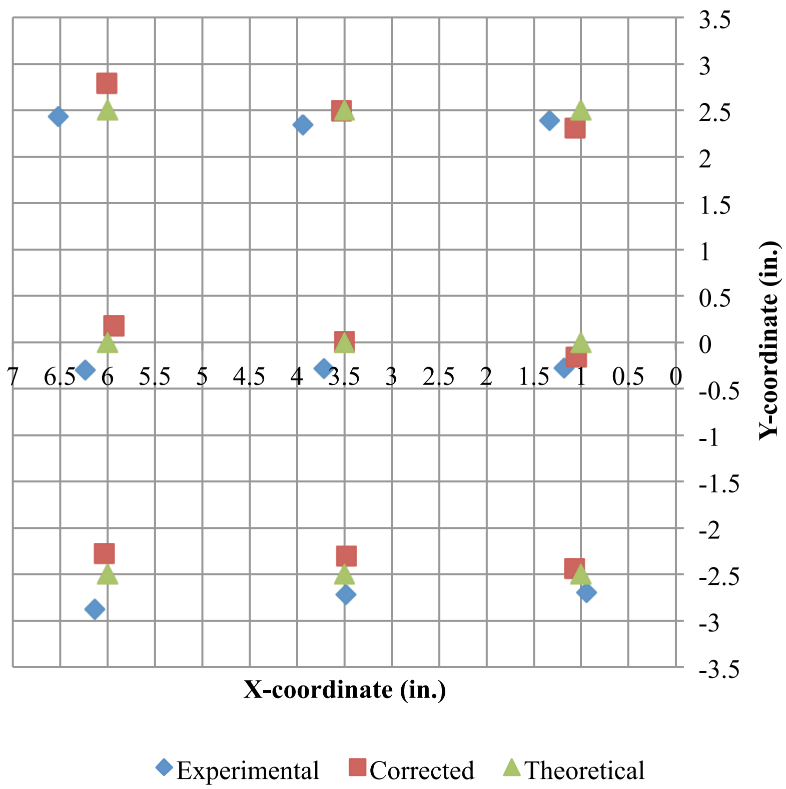

Figure C 2. Plot of theoretical, experimental and corrected points using applied method in Trial 3.

Table C 3. Position errors of experimental and corrected coordinates along with error reduction in Trial 4.

Hole	d_{exp} (in)	d_{corr} (in)	Error reduction
1	0.309	0.174	43.6%
2	0.390	0.130	66.8%
3	0.436	0.150	65.6%
4	0.356	0.066	81.3%
5	0.389	0.075	80.6%
6	0.446	0.207	53.7%
7	0.381	0.278	27.1%
8	0.410	0.078	80.9%
9	0.437	0.246	43.7%
Average	0.395	0.156	60.4%

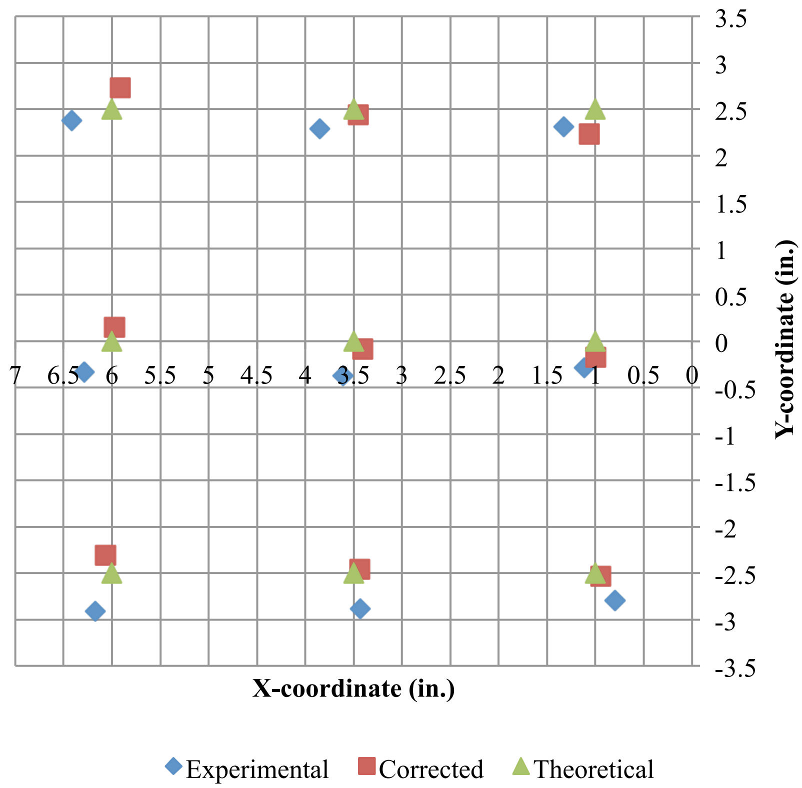

Figure C 3. Plot of theoretical, experimental and corrected points using applied method in Trial 4.

Table C 4. Position errors of experimental and corrected coordinates along with error reduction in Trial 5.

Hole	d_{exp} (in)	d_{corr} (in)	Error reduction
1	0.297	0.141	52.5%
2	0.334	0.028	91.7%
3	0.364	0.250	31.4%
4	0.303	0.034	88.8%
5	0.318	0.109	65.6%
6	0.429	0.237	44.7%
7	0.362	0.180	50.3%
8	0.411	0.031	92.4%
9	0.460	0.326	29.1%
Average	0.364	0.148	60.7%

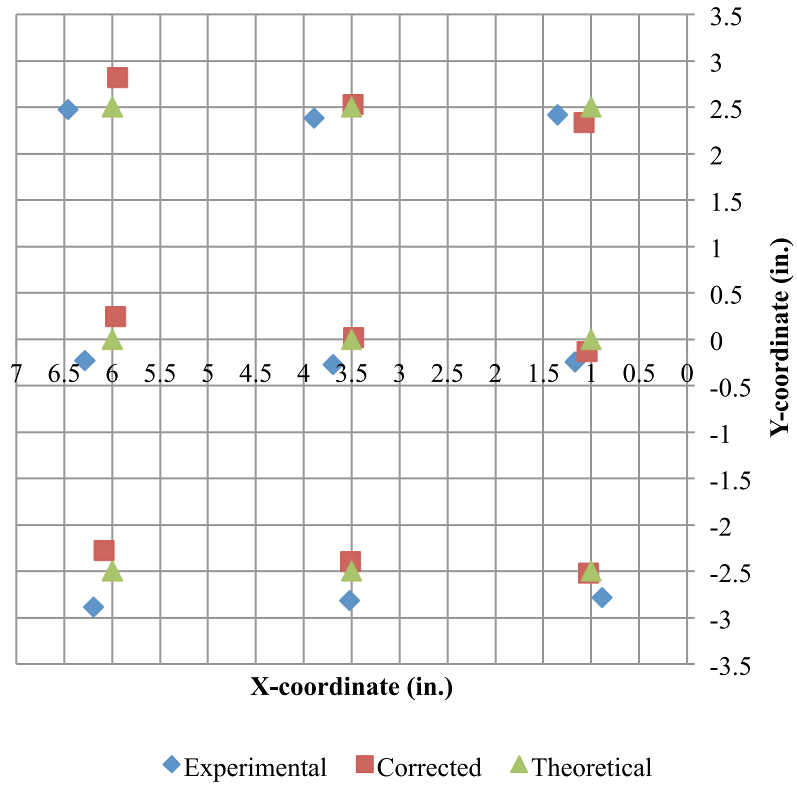

Figure C 4. Plot of theoretical, experimental and corrected points using applied method in Trial 5..

Appendix D. Plots of theoretical, experimental and corrected triangles.

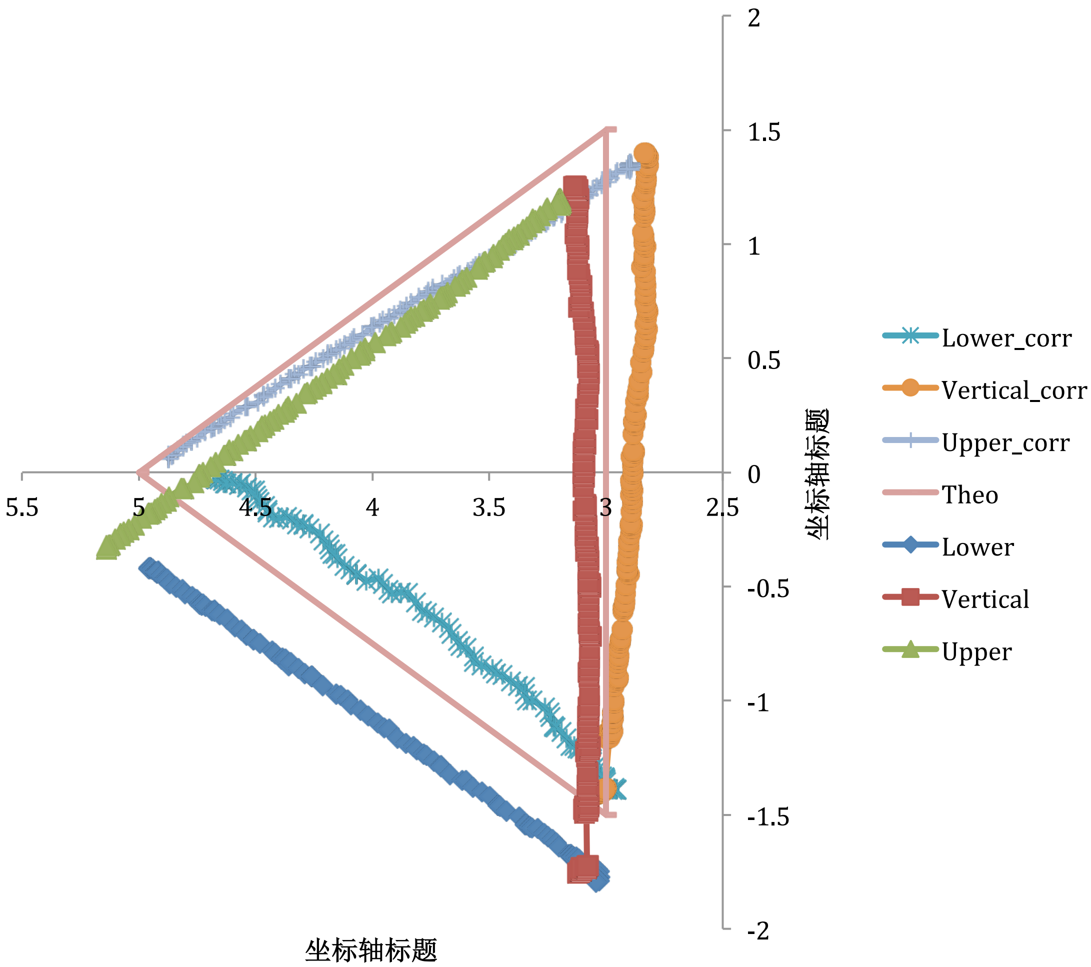

Figure D 1. Plot of theoretical, experimental and theoretical triangles for dynamic testing in Trial 1.

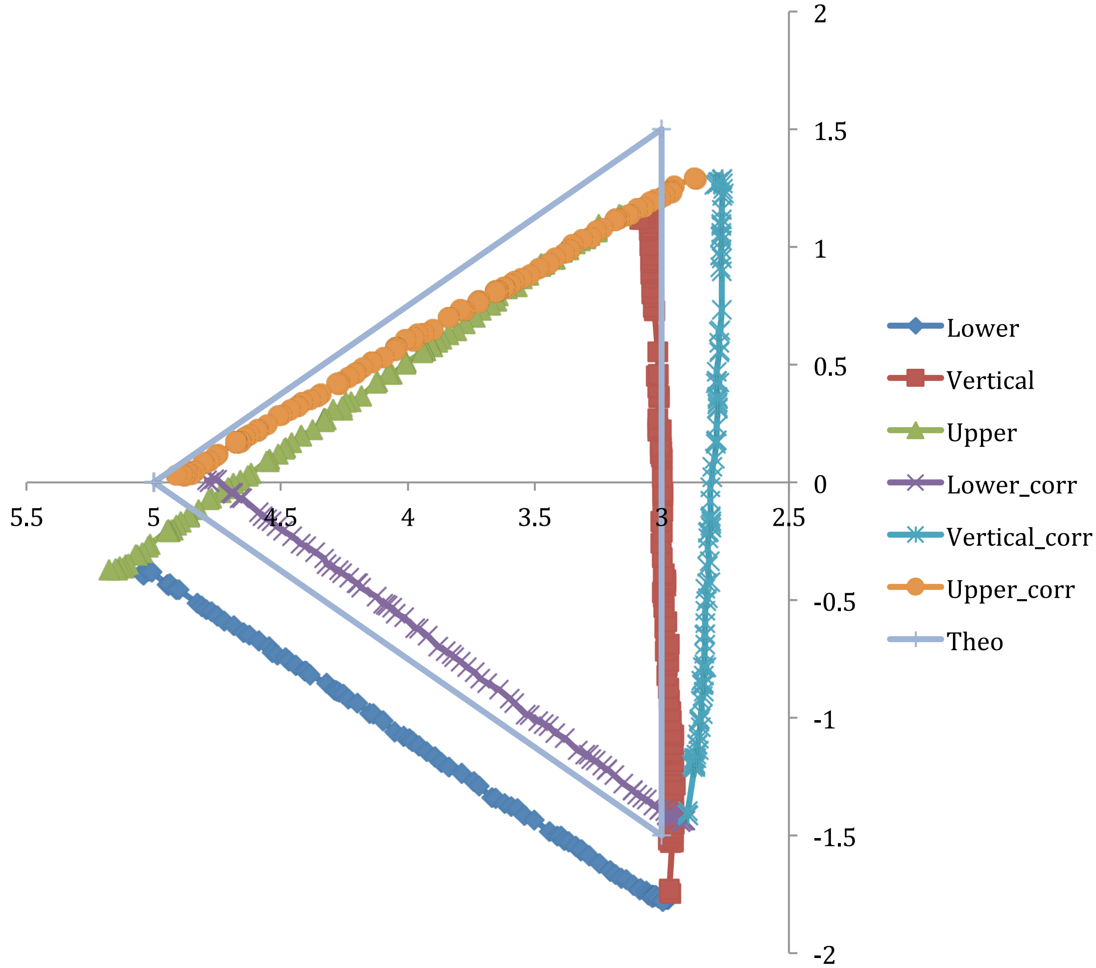

Figure D 2. Plot of theoretical, experimental and theoretical triangles for dynamic testing in Trial 3.

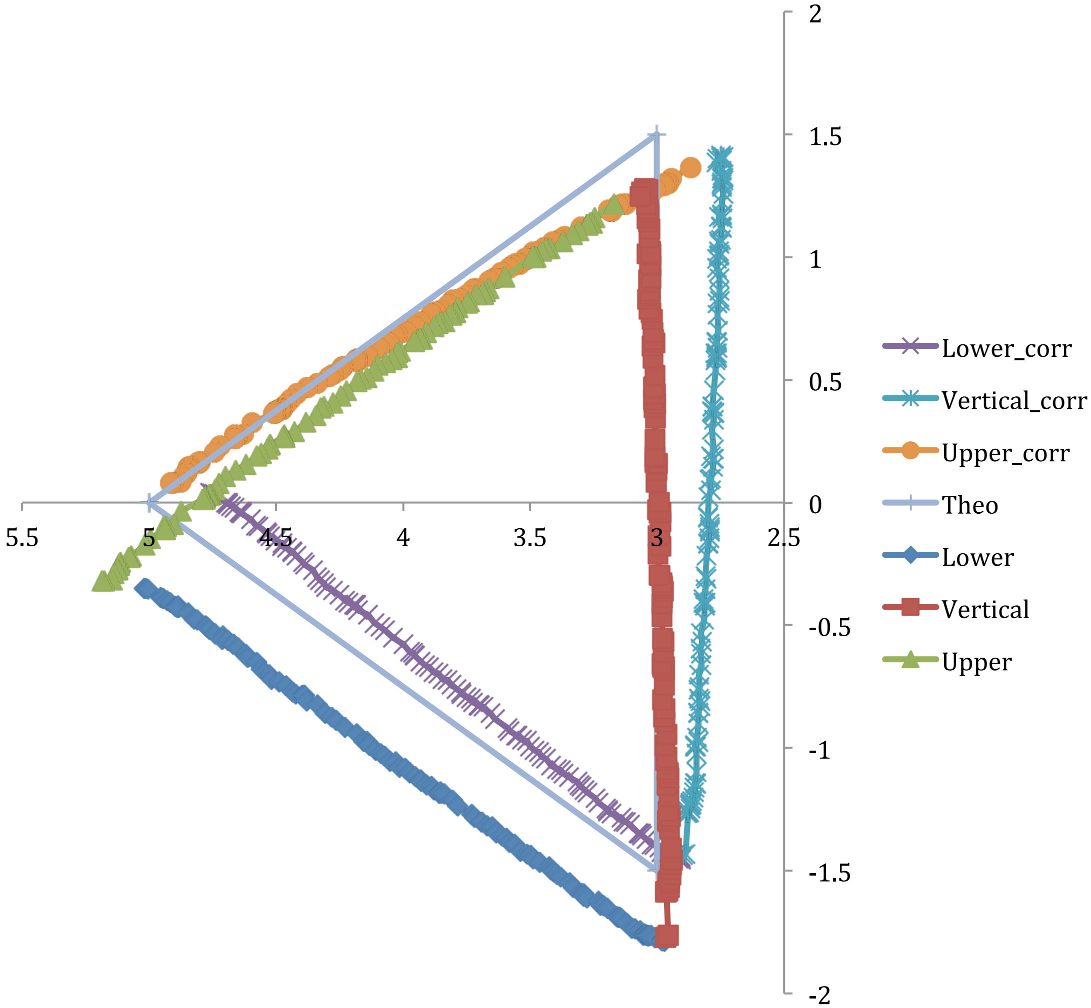

Figure D 3. Plot of theoretical, experimental and theoretical triangles for dynamic testing in Trial 4

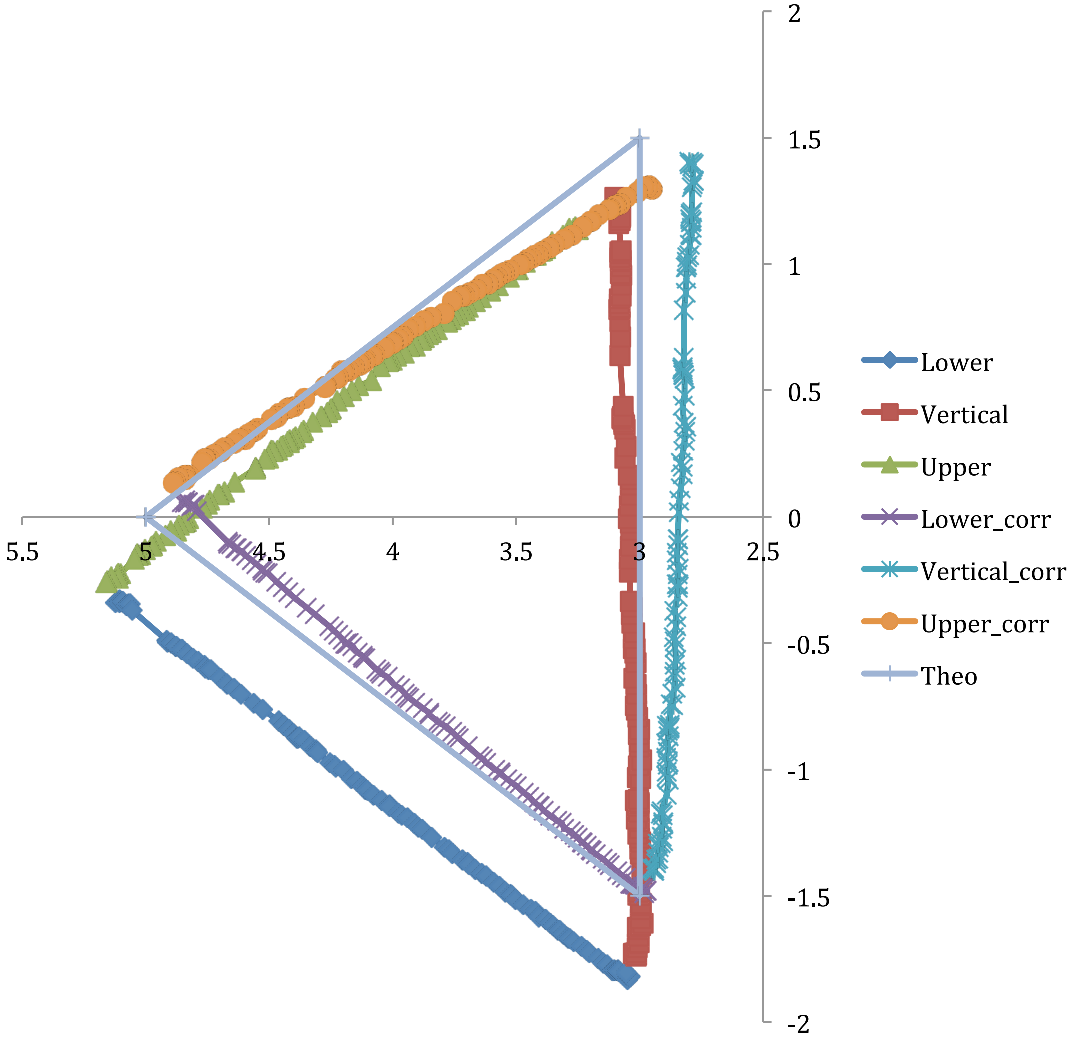

Figure D 4. Plot of theoretical, experimental and theoretical triangles for dynamic testing in Trial 5.